PHYSICAL REVIEW C VOLUME 17, NUMBER 4 APRIL 1978

Nuclear charge distributions deduced from the muonic atoms of ^{232}Th, ^{235}U, ^{238}U, and ^{239}Pu†

D. A. Close, J. J. Malanify, and J. P. Davidson*
University of California, Los Alamos Scientific Laboratory, Los Alamos, New Mexico 87545
(Received 25 October 1977)

The muonic x rays from four highly deformed actinide nuclei, ^{232}Th, ^{235}U, ^{238}U, and ^{239}Pu, have been measured. A four parameter Fermi charge distribution with distortion terms of the form $\beta_{2n} Y_{2n0}$, $n \leq 2$, was used to characterize the nuclear charge distribution. A least squares fit was made to the energies of the $2p$-$1s$ and $3d$-$2p$ muonic x rays and their fine and hyperfine structure splitting. The $4f$-$3d$ and $5g$-$4f$ muonic x rays were measured for the four nuclei as well as the 5-3, 4-2, and 3-1 muonic transitions for ^{232}Th and ^{238}U. The intrinsic electric quadrupole moments were deduced. Our results are compared with those from earlier muonic experiments, as well as with proton, α, and electron inelastic scattering.

[NUCLEAR STRUCTURE Muonic ^{232}Th, ^{235}U, ^{238}U, ^{239}Pu; measured transition energies and relative intensities; deduced nuclear charge parameters in distorted Fermi charge distribution; deduced intrinsic electric quadrupole moments.]

I. INTRODUCTION

It is well known that the muon in muonic atoms is a useful probe of nuclear structure.[1] In particular, for highly deformed nuclei, muonic atoms provide a way to measure the intrinsic quadrupole and, in some cases, hexadecapole moments.[2-4]. The actinides make ideal systems to study because they have high Z (yielding high energy x rays) and because they are highly deformed (yielding complex spectra from the large hyperfine interactions). Indeed, it is interesting to note that in their original papers on the subject, both Wilets[5] and Jacobsohn[6] took as some of their examples the actinide nuclei ^{230}Th, and ^{235}U and ^{238}U, respectively. These theoretical demonstrations that the dynamic quadrupole hyperfine interaction could leave the deformed nucleus in an excited state a significant fraction of the time preceded, by almost a decade, the experimental verification.

The earliest experimental work in the actinide region[7,8] was with NaI detectors and the even-A nuclei ^{232}Th and ^{238}U. A short time later the odd-A nuclei ^{235}U and ^{239}Pu were similarly investigated.[9] While the resolution of the NaI detectors was sufficient to prove the existence of the hyperfine interaction, it was insufficient to reveal the complicated spectra predicted by Wilets and Jacobsohn.

Shortly thereafter these investigations were repeated using Ge(Li) detectors, first using natural uranium targets[10] and then using the four actinides reported here.[11] The even-even muonic atoms of ^{232}Th and ^{238}U have most recently been studied by McKee[12] and Cote *et al.*[13]

With the availability of more intense muon beams it seemed worthwhile to repeat these investigations on the four actinides ^{232}Th, ^{235}U, ^{238}U, and ^{239}Pu. We report here the results of this investigation.[14] In particular, we wanted not only to measure the quadrupole deformations and intrinsic electric quadrupole moments again, hopefully to greater accuracy, but also to see if it was possible to measure the higher deformations and associated intrinsic electric moments.

Section II explains the experimental procedure, including data acquisition and reduction, and Sec. III presents the experimental results. The theory is outlined in some detail in Sec. IV; Sec. V deals with the fitting procedure and other analysis techniques used for extracting the nuclear parameters from the x-ray energies and intensities. The results of this analysis are presented in Sec. VI. Finally, Sec. VII presents a discussion of our results and comparisons with the work of others.

II. EXPERIMENTAL PROCEDURE AND DATA REDUCTION

The data were collected at the 600 MeV synchrocyclotron at the NASA Space Radiation Effects Laboratory (SREL). A thin carbon filament was used as an internal target to produce negative pions. These pions were captured into an alternating gradient channel[15] and were allowed to decay in flight. The backward decaying muons were focused onto a standard beam counter telescope shown in Fig. 1. The beam size was about 200 mm by 200 mm. Counters 1 and 2 were plastic scintillators and served as a beam monitor. The polyethylene absorber was used to slow the muons so as to maximize the number which stopped in the target material. Counters 3 and 3′ were adjacent to and the same size as the targets and defined the incident muon beam; counter 4 was a large area

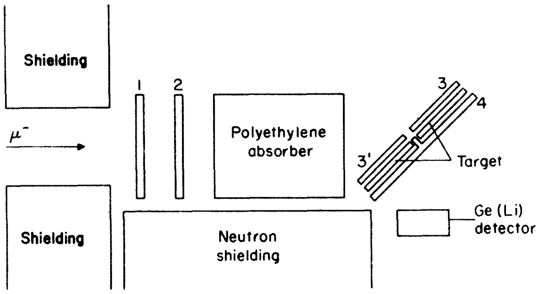

FIG. 1. Block diagram of muon telescope including the position of the Ge(Li) muonic x-ray detector.

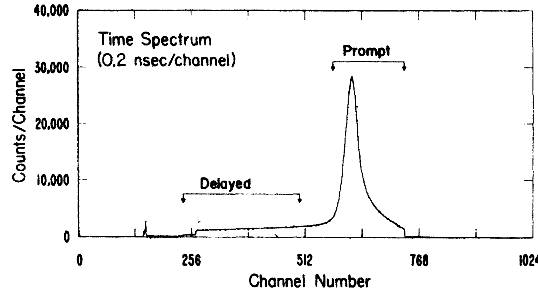

FIG. 2. A typical time spectrum, having a resolving time of about 10 ns.

anticoincidence counter used to define a muon stop. A stopped muon was signified by coincident signals from counters 1, 2, and 3 or 3′, with no signal from counter 4. Muon stopping rates were typically 25 000 per second. The muonic x-ray detector was a large volume (~75 cm^3), high resolution (~1.8 keV at 1.33 MeV and ~7 keV at 6 MeV) Ge(Li) detector.

Table I shows the area, mass, and isotopic purity of the targets. All targets were of pure metallic form. The plutonium target was hermetically sealed by a 0.5 mm thick welded aluminum shell.

The data from the even-even targets (^{232}Th and ^{238}U) correspond to approximately 4×10^9 muon stops while the odd-A target (^{235}U and ^{239}Pu) data correspond to only about 1×10^9 muon stops. The Ge(Li) detector was surrounded by a graded shield to prevent its singles rate from exceeding 10 000 counts per second during data acquisition. This shielding significantly reduced the number of low energy events, particularly for ^{239}Pu.

The analog-to-digital converter (ADC) for the Ge(Li) detector was stabilized both in gain and in zero setting using a precision pulser. Data runs were limited to 6–8 hours with the expectation that small spectral shifts might occur and would be minimized by analyzing the data for short time periods. However, no detectable shifts occurred and runs were simply summed prior to analysis.

The counter telescope permitted the collection of data from two targets simultaneously. One of these targets was the actinide isotope under study while the other target was ^{208}Pb, which provided the energy calibration and detector line shapes.

For each target, three spectra were collected. A 1024 channel spectrum of the time elapsed between the muon stop and the detected muonic x ray permitted time windows to be set such that both an 8192 channel prompt energy spectrum and an 8192 channel delayed energy spectrum were acquired. The energy scale corresponded to 1.1 keV per channel. Figure 2 displays a typical time spectrum for the ^{208}Pb data. A resolving time of ~10 ns was normally achieved for all Ge(Li) events greater than 200 keV. A time window of 3 to 4 times this value defined a prompt event. The delayed time window was typically ~50 ns. The sharp time resolution helped to minimize the number of uncorrelated natural radioactivity events in the prompt energy spectrum, leaving a relatively clean spectrum of muonic x rays. The delayed spectrum permitted us to identify capture γ-ray events as well as the natural radioactivity from the actinide targets. The SREL IBM 360/44 computer was used to collect, sort, and record the data on magnetic tape.

The peaks in the ^{208}Pb muonic x-ray spectrum were fitted to a line shape consisting of a Gaussian function having exponential tails on both sides of the peak.[16] These standard line shapes were then applied to the more complex actinide spectra yielding accurate values for the channel location and the uncertainty in the channel location for all peaks in all spectra. The number of counts in each peak and its uncertainty were also determined.

The energy calibration for the actinide data was provided by the energies of the ^{208}Pb muonic x rays[17] and the accurately known ^{232}Th natural γ-ray lines at 238.6, 583.2, 911.2, and 2614 keV.[18] Our calibration procedure is discussed in detail elsewhere.[17]

TABLE I. Target characteristics.

Target	Area (cm^2)	Mass (g)	Isotopic purity (%)
^{232}Th	174	442.9	100.0
^{235}U	174	669.5	95.6
^{238}U	174	670.9	99.8
^{239}Pu	58	185.1	97.7

III. EXPERIMENTAL RESULTS

The experimental muonic x-ray energies of the electric dipole transitions between "circular" or-

TABLE II. Comparison of ^{232}Th muonic transition energies and relative intensities.

Transition	This experiment[a] Energy (keV)	Rel. int.	Carnegie experiment[b] Energy (keV)	Rel. int.	This calculation Energy (keV)	Rel. int.	Carnegie calculation[b] Energy (keV)	Rel. int.	CERN calculation[c] Energy (keV)	Rel. int.
$2p$–$1s$	*5965.94 ± 0.57	0.012			5965.12	0.011				
	*6021.86 ± 0.52	0.049	6021.5 ± 1.3	0.052	6021.12	0.052	6019.4	0.057	6020.2	0.051
	*6053.30 ± 0.50	0.202	6050.2 ± 0.8	0.189	6053.53	0.171	6050.8	0.186	6052.4	0.182
	*6070.72 ± 0.50	0.250	6067.4 ± 1.0	0.262	6070.87	0.224	6067.8	0.236	6070.0	0.223
	*6077.91 ± 0.51	0.088	6077.2 ± 1.3	0.105	6077.77	0.085	6074.3	0.112	6077.1	0.095
	*6103.16 ± 0.53	0.027	6098.5 ± 1.3	0.042	6103.28	0.035	6099.2	0.037	6102.2	0.037
	*6270.48 ± 0.63	0.010	6272.2 ± 2.6	0.017	6270.77	0.015	6272.3	0.016		
	*6304.72 ± 0.50	0.098	6302.2 ± 0.9	0.097	6304.28	0.091	6302.3	0.102	6305.1	0.090
	*6316.67 ± 0.56	0.018	6313.4 ± 3.3	0.023	6316.89	0.022	6314.3	0.020	6317.5	0.019
	*6353.76 ± 0.50	0.120	6350.5 ± 0.7	0.105	6354.03	0.113	6350.7	0.124	6354.9	0.108
	*6383.14 ± 0.51	0.034	6380.4 ± 1.2	0.040	6383.42	0.042	6378.9	0.041	6384.3	0.040
	*6406.07 ± 0.50	0.062	6403.2 ± 0.9	0.068	6406.07	0.073	6403.8	0.068	6407.3	0.066
	*6455.40 ± 0.50	0.030			6455.82	0.032			6457.1	0.029
$3d$–$2p$	*2740.06 ± 0.38	0.026			2740.34	0.020			2739.3	0.018
	*2795.80 ± 0.39	0.062	2798.2 ± 1.0		2795.88	0.057	2795.3		2794.8	0.056
	*2818.92 ± 0.40	0.042	2820.2 ± 1.7		2818.53	0.034	2820.7		2817.9	0.033
	*2829.60 ± 0.42	0.024	2834.6 ± 1.7		2829.51	0.022	2830.3		2829.2	0.021
	*2865.33 ± 0.45	0.017	2862.0 ± 2.0		2865.60	0.012	2865.3		2865.0	0.018
	2888.30 ± 0.50	0.012								
	*2897.49 ± 0.42	0.046	2903.1 ± 3.0		2897.68	0.040	2897.3		2897.0	0.041
	2906.57 ± 0.52	0.017								
	*2915.16 ± 0.41	0.168	2915.2 ± 0.8		2914.85	0.134	2914.5		2914.5	0.144
	3044.23 ± 0.91	0.002								
	3053.83 ± 0.47	0.009								
	*3092.70 ± 0.48	0.035	3095.3 ± 2.0		3092.88	0.050	3093.8		3094.3	0.047
	3118.32 ± 0.69	0.028								
					3124.18	0.045			3125.1	0.043
	*3125.07 ± 0.46	0.310	3124.8 ± 0.7		3125.29	0.296	3125.2		3126.4	0.274
	*3141.68 ± 0.49	0.066	3140.1 ± 1.5		3141.36	0.052	3142.6		3142.5	0.057
	*3148.83 ± 0.47	0.137	3148.6 ± 1.2		3148.43	0.159	3149.1		3149.8	0.158
					3151.84	0.011				
$4f$–$3d$	1074.45 ± 0.25	0.038			1073.44	0.022				
	1113.63 ± 0.74	0.014								
	1126.27 ± 0.09	0.256	1125.8 ± 1.1	0.286	1125.98	0.201	1127.01	0.256		
					1126.32	0.020				
					1129.73	0.019				
	1143.85 ± 0.09	0.322	1143.3 ± 1.1	0.371	1143.15	0.331	1144.2	0.333		
	1185.74 ± 0.10	0.370	1185.7 ± 1.1	0.343	1185.27	0.393	1185.9	0.410		
$5g$–$4f$					516.75	0.015				
	520.81 ± 0.06	0.568	520.5 ± 0.3	0.583	520.80	0.550	520.79	0.565		
	530.20 ± 0.07	0.432	530.3 ± 0.3	0.417	530.18	0.433	530.18	0.435		

[a] Those energies marked with an asterisk (*) were used to determine the nuclear charge parameters.
[b] See Ref. 13.
[c] See Ref. 11.

TABLE III. Comparison of ^{235}U muonic transition energies and relative intensities.

	This experiment [a]		This calculation		CERN calculation [b]	
Transition	Energy (keV)	Rel. int.	Energy (keV)	Rel. int.	Energy (keV)	Rel. int.
$2p-1s$	6112.45 ± 2.45	0.009				
			6117.76	0.010	6118.7	0.018
	*6119.86 ± 1.40	0.020	6121.71	0.018	6121.1	0.017
	*6150.11 ± 0.87	0.035	6150.63	0.025		
	*6158.09 ± 1.26	0.078	6157.57	0.054	6156.9	0.057
	*6165.23 ± 1.22	0.211	6163.96	0.131	6163.2	0.136
			6167.91	0.139	6167.1	0.142
	*6169.77 ± 1.15	0.118	6170.83	0.049		
					6175.7	0.054
					6181.8	0.020
	*6205.82 ± 0.86	0.029	6203.77	0.016		
			6207.43	0.011		
	*6397.96 ± 1.18	0.023	6397.77	0.020	6395.8	0.020
			6414.37	0.015	6413.3	0.026
	*6414.65 ± 1.17	0.048	6415.15	0.028		
	*6453.06 ± 1.31	0.042	6454.57	0.023	6452.8	0.022
			6460.57	0.090	6458.6	0.087
	*6460.36 ± 1.24	0.215	6461.34	0.015		
			6461.35	0.104	6459.3	0.098
			6484.63	0.013		
	*6501.63 ± 1.36	0.033	6500.77	0.032	6498.8	0.030
					6523.1	0.019
	*6544.28 ± 1.39	0.024	6546.23	0.014		
	*6557.36 ± 1.45	0.098	6558.58	0.085	6556.4	0.082
	*6587.44 ± 2.82	0.018	6587.63	0.013		
$3d-2p$	*2910.80 ± 0.42	0.022	2910.96	0.016		
	*2946.48 ± 0.40	0.036	2945.69	0.022	2946.7	0.025
	*2959.47 ± 0.38	0.044	2960.28	0.030	2961.4	0.037
	*2984.86 ± 0.46	0.028	2984.28	0.015		
	*2997.44 ± 0.37	0.062	2997.81	0.053	2998.7	0.055
	3016.54 ± 0.80	0.022				
			3021.24	0.036	3022.0	0.037
	*3023.52 ± 0.79	0.171	3022.03	0.024	3022.7	0.025
			3025.13	0.067	3026.1	0.069
			3031.86	0.010		
	*3032.21 ± 0.46	0.051	3032.65	0.021	3033.5	0.022
	*3043.73 ± 0.44	0.041	3043.71	0.027	3044.5	0.030
	*3211.42 ± 0.52	0.018	3212.03	0.015	3212.7	0.026
	*3224.93 ± 0.51	0.022	3225.29	0.026	3225.2	0.024
	*3242.06 ± 0.52	0.096	3241.96	0.063	3241.7	0.056
			3244.96	0.033		
	*3246.67 ± 0.58	0.124	3245.91	0.052	3245.6	0.046
			3247.63	0.028	3247.4	0.025
	*3252.64 ± 0.53	0.070	3251.58	0.050	3251.3	0.045
			3259.18	0.014		
	*3260.47 ± 0.45	0.090	3261.15	0.066	3261.0	0.063
			3265.03	0.014	3263.8	0.023
	3267.56 ± 0.50	0.035	3269.45	0.021		
			3275.44	0.016		
	*3281.21 ± 0.45	0.050	3280.89	0.036	3280.7	0.037
	3317.87 ± 0.55	0.015				
$4f-3d$			1162.88	0.015		
			1173.91	0.020		
			1175.87	0.023		
			1178.00	0.013		
	1181.16 ± 0.18	0.241	1181.41	0.101		
			1183.23	0.021		
			1184.97	0.017		

TABLE III. (Continued)

Transition	This experiment [a] Energy (keV)	Rel. int.	This calculation Energy (keV)	Rel. int.	CERN calculation [b] Energy (keV)	Rel. int.
			1189.14	0.021		
			1190.10	0.074		
	1191.63 ± 0.16	0.270	1193.03	0.052		
			1193.84	0.027		
			1197.23	0.017		
			1198.97	0.013		
			1207.79	0.024		
			1212.68	0.014		
			1217.75	0.014		
	1219.42 ± 0.45	0.069	1220.28	0.024		
			1222.69	0.022		
			1232.20	0.026		
	1236.28 ± 0.20	0.155	1236.02	0.097		
			1245.38	0.036		
			1247.05	0.036		
			1249.59	0.016		
	1250.80 ± 0.17	0.265	1251.05	0.040		
			1251.39	0.071		
			1252.73	0.010		
$5g$-$4f$			540.69	0.025		
			542.29	0.042		
			542.43	0.127		
	544.68 ± 0.09	0.557	544.24	0.060		
			545.84	0.112		
			545.98	0.078		
			546.80	0.096		
			550.46	0.026		
			552.87	0.044		
			552.92	0.115		
	555.08 ± 0.09	0.443	555.40	0.063		
			556.74	0.101		
			557.07	0.082		

[a] Those energies marked with an asterisk (*) were used to determine the nuclear charge parameters.
[b] See Ref. 11.

bits, $2p$-$1s$, $3d$-$2p$, $4f$-$3d$, and $5g$-$4f$, are listed in Tables II–V for ^{232}Th, ^{235}U, ^{238}U, and ^{239}Pu, respectively. Also listed is the observed relative intensity of each line within a major transitional group. This intensity information was used only to verify the correspondence of a calculated transition with the observed experimental line. The calculated energies and relative intensities which result from the data analysis to be described later are also presented in Tables II–V.

The experimental and calculational results of Coté *et al.*[13] for ^{232}Th and ^{238}U are also shown for comparison in Tables II and IV. It would be appropriate to compare our experimental energies with those of McKee[12] for ^{232}Th and ^{238}U and DeWit *et al.*[11] for ^{232}Th, ^{235}U, ^{238}U, and ^{239}Pu. However, these authors did not report their data in tabular form, thus preventing a detailed comparison. The tabulated calculational results of the CERN work[11] are available and are shown for comparison purposes in Tables II–V. Our results agree quite well with the earlier results for the $3d$-$2p$, $4f$-$3d$, and $5g$-$4f$ transitions. For the $2p$-$1s$ transitions, our energies appear to be 2 to 4 keV higher than Coté *et al.* However, we are in good agreement with the calculated results of DeWit *et al.*

Figures 3–5 display our experimental spectra for the $2p$-$1s$, $3d$-$2p$, and $4f$-$3d$ transitions, respectively. These figures can be compared with those in Refs. 11–13 to confirm that the present experiment is of improved counting statistics and energy resolution.

Figure 3 shows not only the elemental shift in the x-ray energies, but also the isotopic shift in the energies. Also seen is the change in the character of the spectrum between elements and isotopes. The $2p$-$1s$ spectra from the two even-even nuclei are almost identical in shape, which is ex-

TABLE IV. Comparison of ^{238}U muonic transition energies and relative intensities.

Transition	This experiment[a] Energy (keV)	Rel. int.	Carnegie experiment[b] Energy (keV)	Rel. int.	This calculation Energy (keV)	Rel. int.	Carnegie calculation[b] Energy (keV)	Rel. int.	CERN calculation[c] Energy (keV)	Rel. int.
$2p$–$1s$	6047.36 ± 0.49	0.024			6045.58	0.015				
	*6096.58 ± 0.32	0.056	6093.5 ± 1.7	0.066	6095.79	0.059	6092.6	0.065	6096.9	0.057
					6105.50	0.016			6106.4	0.019
	*6122.10 ± 0.30	0.163	6119.2 ± 0.8	0.187	6122.59	0.153	6119.1	0.177	6123.5	0.157
	*6140.46 ± 0.30	0.220	6136.5 ± 1.2	0.198	6140.79	0.196	6137.3	0.216	6141.6	0.195
	*6149.03 ± 0.32	0.089	6145.0 ± 1.7	0.138	6148.98	0.087	6145.6	0.109	6149.9	0.098
	*6167.41 ± 0.35	0.031	6162.1 ± 1.7	0.035	6167.59	0.035	6163.8	0.040	6168.2	0.035
	*6379.26 ± 0.47	0.015			6378.62	0.018				
	*6409.44 ± 0.34	0.112	6407.3 ± 0.7	0.124	6409.38	0.118	6406.8	0.131	6410.6	0.121
	*6416.50 ± 0.50	0.029			6417.39	0.023			6418.5	0.020
	*6454.14 ± 0.35	0.113	6451.0 ± 0.7	0.118	6454.38	0.120	6451.5	0.133	6455.3	0.120
	6462.62 ± 0.63	0.021								
	6480.93 ± 0.36	0.033	6476.8 ± 2.0	0.021	6482.02	0.034	6479.1	0.036	6483.1	0.031
	*6518.36 ± 0.33	0.064	6514.3 ± 0.8	0.068	6518.19	0.061	6515.7	0.061	6519.5	0.055
	*6563.70 ± 0.50	0.032	6561.7 ± 1.1	0.045	6563.19	0.032	6560.4	0.032	6564.2	0.029
$3d$–$2p$	*2826.66 ± 0.24	0.021			2826.42	0.020			2827.0	0.018
	*2882.88 ± 0.23	0.044			2883.01	0.036			2883.5	0.034
	*2919.50 ± 0.32	0.046			2919.18	0.031			2919.9	0.028
	*2927.12 ± 0.44	0.030			2927.22	0.023			2928.0	0.021
	*2956.92 ± 0.37	0.018			2957.30	0.016			2958.0	0.024
	2994.77 ± 0.89	0.023								
	*3013.02 ± 0.25	0.286	3012.8 ± 0.8		3012.77	0.201	3011.7		3013.2	0.223
	*3191.54 ± 0.93	0.021			3192.30	0.013				
	*3221.86 ± 0.44	0.039	3220.8 ± 1.0		3222.02	0.062	3221.6		3223.0	0.057
	*3249.08 ± 0.27	0.306	3249.7 ± 0.8		3248.81	0.274	3248.1		3249.6	0.249
					3252.22	0.046	3251.7		3253.1	0.043
			3272.6 ± 1.4		3273.17	0.055	3272.8		3273.9	0.061
	*3277.44 ± 0.30	0.166	3279.7 ± 1.4		3278.61	0.121	3278.2		3279.5	0.110
					3281.29	0.015	3281.0		3281.9	0.019
$4f$–$3d$	1127.95 ± 0.09	0.053			1127.33	0.031				
	1181.07 ± 0.08	0.319	1181.1 ± 0.6	0.325	1180.67	0.274	1181.1	0.328		
					1184.26	0.030				
					1186.94	0.015				
	1202.35 ± 0.08	0.245	1202.3 ± 0.6	0.253	1201.62	0.245	1202.3	0.266		
	1243.94 ± 0.06	0.382	1244.0 ± 0.6	0.422	1243.53	0.381	1244.3	0.407		
$5g$–$4f$					540.19	0.015				
	544.42 ± 0.06	0.549	544.6 ± 0.5	0.545	544.62	0.548	544.52	0.565		
	554.75 ± 0.06	0.451	554.5 ± 0.5	0.455	554.88	0.432	554.78	0.435		

[a] Those energies marked with an asterisk (*) were used to determine the nuclear charge parameters. [b] See Ref. 13. [c] See Ref. 11.

TABLE V. Comparison of ^{239}Pu muonic transition energies and relative intensities.

Transition	This experiment [a] Energy (keV)	Rel. int.	This calculation Energy (keV)	Rel. int.	CERN calculation [b] Energy (keV)	Rel. int.
$2p-1s$	*6200.72 ± 0.92	0.036	6201.95	0.030	6199.0	0.031
	*6233.13 ± 0.96	0.163	6231.07	0.028	6227.3	0.028
			6234.62	0.095	6231.0	0.105
			6239.59	0.012		
	*6243.97 ± 0.66	0.121	6243.33	0.071	6239.8	0.063
			6247.44	0.028	6244.0	0.026
	*6250.83 ± 0.79	0.079	6251.18	0.031	6247.8	0.027
			6251.37	0.028	6248.0	0.029
	*6259.56 ± 0.57	0.158	6259.22	0.093	6256.0	0.096
			6259.83	0.035	6256.7	0.033
	6268.11 ± 0.81	0.070	6265.86	0.032	6262.9	0.037
	*6293.60 ± 1.25	0.042	6291.88	0.024	6288.0	0.026
			6298.93	0.010		
			6536.45	0.032	6537.4	0.033
	*6537.39 ± 0.69	0.070	6536.89	0.014		
			6543.25	0.016	6543.7	0.022
	*6560.61 ± 0.70	0.064	6561.05	0.077	6561.6	0.065
	*6567.75 ± 1.06	0.044	6568.90	0.046	6569.6	0.039
	*6593.43 ± 0.71	0.056	6593.72	0.035	6594.4	0.035
			6604.75	0.012		
			6616.81	0.017		
	6661.48 ± 0.72	0.047	6663.17	0.028	6664.8	0.025
			6682.49	0.010		
	6686.68 ± 0.75	0.051	6687.92	0.025	6689.3	0.024
			6690.34	0.012		
$3d-2p$	*2973.63 ± 0.74	0.037	2973.06	0.024	2972.2	0.023
			3019.42	0.017		
	3043.88 ± 0.56	0.014			3042.9	0.017
	*3100.09 ± 0.98	0.033	3099.78	0.023	3099.5	0.021
	*3123.37 ± 2.00	0.119	3121.81	0.018		
			3125.63	0.014	3125.8	0.018
	3133.11 ± 0.42	0.185	3131.34	0.106	3131.0	0.098
					3134.0	0.020
	*3334.58 ± 1.01	0.047	3336.43	0.024	3340.8	0.022
			3360.63	0.012		
			3368.65	0.062	3372.5	0.045
	*3369.81 ± 0.38	0.378	3369.09	0.151	3372.9	0.136
			3370.37	0.023	3374.0	0.021
			3372.38	0.039	3376.3	0.029
			3377.14	0.011		
			3396.22	0.010		
	*3402.44 ± 0.44	0.150	3401.61	0.096	3406.0	0.090
			3404.69	0.012		
			3408.75	0.013		
			3412.57	0.012	3417.0	0.017
			3432.56	0.011		
	3451.14 ± 0.41	0.036	3449.07	0.024	3452.8	0.019
$4f-3d$			1213.53	0.018		
	1229.12 ± 0.28	0.086	1227.53	0.053		
			1231.35	0.044		
	1246.20 ± 0.20	0.196	1246.57	0.175		
	1254.04 ± 0.18	0.233	1253.38	0.186		
			1274.44	0.014		
	1278.19 ± 0.50	0.034	1278.90	0.022		
			1285.47	0.011		
	1303.01 ± 0.18	0.302	1302.51	0.215		
	1310.94 ± 0.20	0.150	1310.48	0.114		

TABLE V. (Continued)

Transition	This experiment[a]		This calculation		CERN calculation[b]	
	Energy (keV)	Rel int.	Energy (keV)	Rel. int.	Energy (keV)	Rel. int.
$5g$-$4f$			559.35	0.016		
	569.18 ± 0.21	0.574	569.13	0.299		
			569.20	0.214		
			570.82	0.015		
			574.68	0.010		
	580.53 ± 0.21	0.426	580.36	0.246		
			580.88	0.165		

[a] Those energies marked with an asterisk (*) were used to determine the nuclear charge parameters.
[b] See Ref. 11.

pected since the nuclear structure for ^{232}Th and ^{238}U is similar. The $2p$-$1s$ spectra from the two odd-A nuclei have a more complicated structure, with the $2p$-$1s$ spectrum from ^{239}Pu being more fractured than that for ^{235}U. The $3d$-$2p$ spectra, Fig. 4, show the same general features as do the $2p$-$1s$ spectra.

Figure 5 shows there is very little hyperfine structure splitting for the $4f$-$3d$ spectra in ^{232}Th and ^{238}U. There are basically three x rays, which is expected from simple fine structure splitting arguments. There appears to be significant hyperfine splitting for the $4f$-$3d$ transitions in ^{235}U and ^{239}Pu.

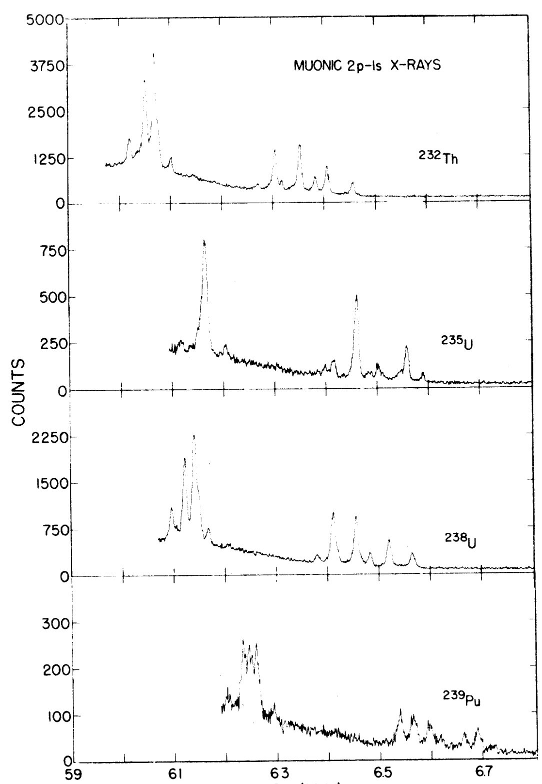

FIG. 3. Composite spectra showing the muonic $2p$-$1s$ transitions in ^{232}Th, ^{235}U, ^{238}U, and ^{239}Pu. Only the full energy peaks are shown. The elemental shift in energy is clearly displayed. The isotope energy shift is also seen in ^{235}U and ^{238}U.

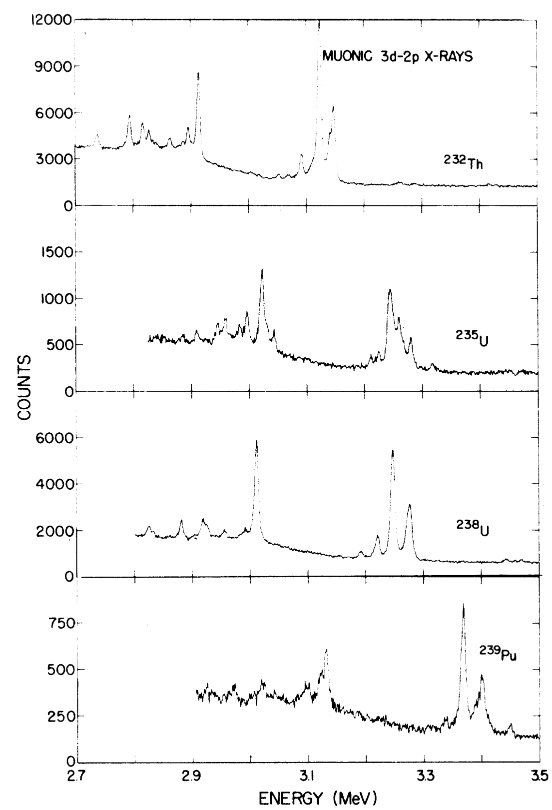

FIG. 4. Spectra showing the $3d$-$2p$ muonic x-ray transitions in the four actinide nuclei. Only the full energy peaks are shown. Elemental and isotope energy shifts are clearly shown.

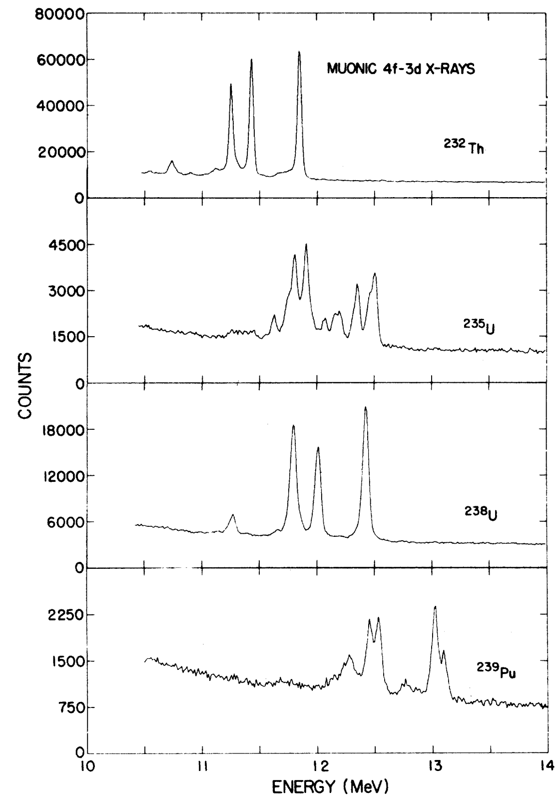

FIG. 5. Muonic $4f$-$3d$ transitions in ^{232}Th, ^{235}U, ^{238}U, and ^{239}Pu. The difference in muonic transitions in an even-even nucleus compared to those in an odd-A nucleus are clearly seen.

It has already been pointed out[19] that these properties of muonic x rays from high-Z targets hold promise for an isotopic as well as elemental materials analysis technique.

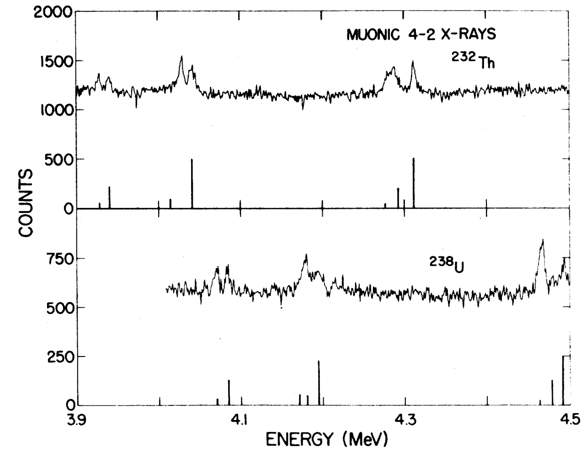

FIG. 7. Muonic 4-2 transitions in ^{232}Th and ^{238}U. Shown for comparison is the calculated $4f$-$2p$ spectrum for each nucleus.

Figures 6–8 display our experimental spectra for the 5-3, 4-2, and $3d$-$1s$ transitions, respectively, for the even-even isotopes ^{232}Th and ^{238}U. The data from the odd-A isotopes were insufficient to clearly observe these transitions. Also shown in Figs. 6–8 are the calculated energies and relative intensities for the $5g$-$3d$, $4f$-$2p$, and $3d$-$1s$ electric quadrupole transitions which result from the fitted parameters to be described later. It is not surprising that in these two even-even actinide nuclei the 5-3, 4-2, and $3d$-$1s$ transitions are very similar in shape, differing mainly in a shift in the energy.

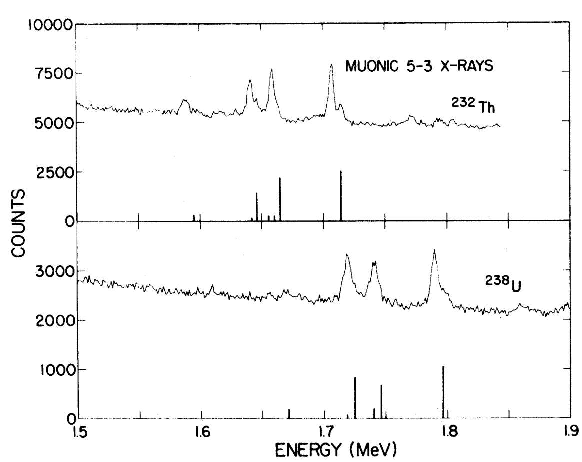

FIG. 6. The 5-3 muonic transitions in ^{232}Th and ^{238}U. Shown for comparison is the calculated $5g$-$3d$ spectrum for each nucleus.

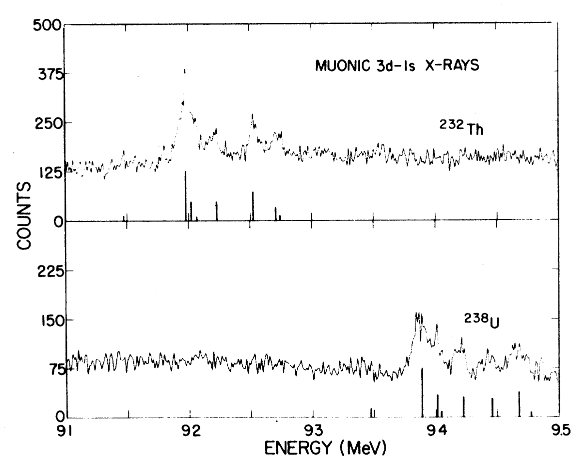

FIG. 8. Muonic $3d$-$1s$ electric quadrupole transitions in ^{232}Th and ^{238}U. The calculated $3d$-$1s$ spectrum for each nucleus is shown for comparison.

IV. THEORY

A. Monopole interaction

1. Dirac solutions

The Hamiltonian which describes the muonic atom is

$$H = H_N + H_\mu + H_{\text{int}} \ , \tag{1}$$

where H_N is the nuclear Hamiltonian in the absence of the muon, H_μ is the muon Hamiltonian with a spherically symmetric potential $V_0(r)$, while H_{int} represents the muon-nucleus interaction minus $V_0(r)$. The eigenfunctions and eigenvalues of the muonic atom are obtained by solving the Dirac equation[20]

$$\frac{d}{dr}\begin{bmatrix} G(r) \\ F(r) \end{bmatrix} = \begin{bmatrix} \dfrac{-\kappa}{r} & W + mc^2 - V_0(r) \\ -W + mc^2 + V_0(r) & \dfrac{\kappa}{r} \end{bmatrix} \begin{bmatrix} G(r) \\ F(r) \end{bmatrix} \ , \tag{2}$$

where $G(r)$ and $F(r)$ are the large and small components, respectively, of the Dirac radial wave function. Their normalization is

$$\int_0^\infty (F^2 + G^2) dr = 1 \ . \tag{3}$$

The muon total energy is W, its reduced mass is m, while the quantum number κ is related to the muon total and orbital angular momenta j and l in the usual nonrelativistic approximation by

$$\kappa = \begin{cases} -l - 1, & j = l + \frac{1}{2} \\ l, & j = l - \frac{1}{2} \ . \end{cases} \tag{4}$$

The interaction between the muon and the nucleus is the Coulomb potential

$$V(\vec{r}_\mu) = -e_\mu \sum_{i=1}^{Z} \frac{e_i}{|\vec{r}_\mu - \vec{r}_i|} = -e^2 \int \frac{\rho(\vec{r})}{|\vec{r}_\mu - \vec{r}|} d^3 r \ . \tag{5}$$

The last expression arises upon passing to the limit of a continuous charge distribution. Clearly $\rho(\vec{r})$ must satisfy

$$e \int \rho(\vec{r}) d^3 r = Ze \ . \tag{6}$$

For the lower lying states of deformed nuclei it is sufficient to take $\rho(\vec{r})$ axially symmetric so that expanding in spherical harmonics[21]

$$\rho(\vec{r}) = \rho_0(r) + \rho_2(r) Y_{20}(\theta, \phi) + \rho_4(r) Y_{40}(\theta, \phi) + \cdots \ . \tag{7}$$

At this point a model assumption is made about the nuclear charge distribution:

$$\rho(\vec{r}) = N \left\{ 1 + \exp\left[\left[r - c \left(1 + \sum_{n=1} \beta_{2n} Y_{2n0}(\theta, \phi) \right) \right] \Big/ a \right] \right\}^{-1} \ , \tag{8}$$

with $n \leq 2$, a form that has been used before.[2] This is a generalization to higher order deformations of the charge distribution used by the Columbia group[22] and is identical to first order to the modified Fermi-type charge distributions used elsewhere.[11,23] The charge distribution parameters are the half density radius $c(1 + \sum_{n=1} \beta_{2n} Y_{2n0})$, which varies with polar angle, the skin thickness $t = 4a \ln 3$, and the deformation parameters β_{2n}. The monopole part of the charge distribution of Eq. (8) is simply the integral over the solid angle of $\rho(\vec{r})$,

$$\rho_0(r) = \frac{1}{4\pi} \int \rho(\vec{r}) d\Omega \ , \tag{9a}$$

while the lth harmonic is

$$\rho_l(r) = \int \rho(\vec{r}) Y_{l0}^*(\theta, \phi) d\Omega \ . \tag{9b}$$

Making use of the usual spherical harmonic expansion of $|\vec{r} - \vec{r}'|^{-1}$, a generalized penetration function $f_l(r_\mu)$ can be defined by

$$\mathcal{E}_l f_l(r_\mu) = \left(\frac{16\pi}{2l+1} \right)^{1/2} \left(\frac{1}{r_\mu^{l+1}} \int_0^{r_\mu} \rho_l(r) r^{l+2} dr + r_\mu^l \int_{r_\mu}^\infty \rho_l(r) r^{-l+1} dr \right) \ . \tag{10}$$

The quantity $\mathcal{E}_l$ is the generalized intrinsic electric multipole moment. With these definitions, the potential of Eq. (5) becomes

$$V(\vec{r}_\mu) = \sum_{l'=0} V_{l'}(\vec{r}_\mu) \ , \tag{11}$$

l' even. The spherically symmetric part of the potential is

$$V_0(r_\mu) = -4\pi e^2 \left(\frac{1}{r_\mu} \int_0^{r_\mu} \rho_0(r') r'^2 dr' + \int_{r_\mu}^\infty \rho_0(r') r' dr' \right) \ , \tag{11a}$$

and the higher order terms are

$$V_l(\vec{r}_\mu) = -\tfrac{1}{2} e^2 \mathcal{E}_l f_l(r_\mu) P_l(\cos\theta) = -\tfrac{1}{2} e^2 \mathcal{E}_l f_l(r_\mu) \left(\frac{4\pi}{2l+1} Y_{l0}(\theta_\mu, \phi_\mu) Y_{l0}(\theta_N, \phi_N) \right) \ . \tag{11b}$$

TABLE VI. Muonic level energies and corrections (keV) using the parameters obtained from a best fit to the experimental data. Dirac is the calculated level location. $E_{VP}^{(1)}$ is the first order vacuum polarization correction. E_{LS} is the Lamb shift correction. $E_{VP}^{(h)}$ is the higher order vacuum polarization correction. E_{RR} is the relativistic recoil correction. E_{ES} is the electron screening correction. E_{NP} is the nuclear polarization correction. A positive correction implies more binding. These values do not include the quadrupole or hexadecapole interaction.

Level	Calculation	^{232}Th	^{235}U	^{238}U	^{239}Pu
$1s_{1/2}$	Dirac	11 755.831	12 101.404	12 072.085	12 436.279
	$E_{VP}^{(1)}$	72.988	74.985	74.710	76.831
	E_{LS}	−2.768	−2.805	−2.780	−2.829
	$E_{VP}^{(h)}$	−0.647	−0.691	−0.691	−0.738
	E_{RR}	0.406	0.420	0.412	0.431
	E_{ES}	0.009	0.011	0.011	0.012
	E_{NP}	6.100	6.800	6.400	6.100
$2p_{1/2}$	Dirac	5 668.704	5 903.009	5 897.420	6 138.402
	$E_{VP}^{(1)}$	37.559	39.211	39.119	40.841
	E_{LS}	−0.436	−0.463	−0.462	−0.491
	$E_{VP}^{(h)}$	−0.479	−0.517	−0.517	−0.558
	E_{RR}	0.138	0.148	0.146	0.157
	E_{ES}	0.021	0.024	0.024	0.027
	E_{NP}	1.800	2.000	1.900	1.800
$2p_{3/2}$	Dirac	5 452.095	5 676.108	5 672.001	5 901.754
	$E_{VP}^{(1)}$	34.684	36.228	36.161	37.764
	E_{LS}	−0.842	−0.892	−0.889	−0.942
	$E_{VP}^{(h)}$	−0.464	−0.500	−0.500	−0.539
	E_{RR}	0.120	0.129	0.127	0.137
	E_{ES}	0.022	0.026	0.026	0.029
	E_{NP}	1.800	2.000	1.900	1.800
$3d_{3/2}$	Dirac	2 617.668	2 738.676	2 738.508	2 862.487
	$E_{VP}^{(1)}$	12.467	13.268	13.263	14.096
	E_{LS}	0.061	0.065	0.064	0.068
	$E_{VP}^{(h)}$	−0.273	−0.299	−0.299	−0.327
	E_{RR}	0.021	0.023	0.023	0.025
	E_{ES}	0.058	0.065	0.065	0.073
	E_{NP}	−0.030	−0.031	−0.029	−0.030
$3d_{5/2}$	Dirac	2 557.843	2 673.692	2 673.607	2 792.090
	$E_{VP}^{(1)}$	11.515	12.230	12.228	12.968
	E_{LS}	−0.079	−0.088	−0.088	−0.097
	$E_{VP}^{(h)}$	−0.263	−0.288	−0.288	−0.315
	E_{RR}	0.019	0.021	0.020	0.022
	E_{ES}	0.061	0.068	0.068	0.077
	E_{NP}	0.0	0.0	0.0	0.0
$4f_{5/2}$	Dirac	1 446.456	1 512.568	1 512.576	1 580.236
	$E_{VP}^{(1)}$	3.862	4.154	4.154	4.459
	E_{LS}	0.019	0.021	0.021	0.023
	$E_{VP}^{(h)}$	−0.145	−0.160	−0.160	−0.176
	E_{RR}	0.005	0.006	0.005	0.006
	E_{ES}	0.135	0.150	0.150	0.166
	E_{NP}	0.0	0.0	0.0	0.0
$4f_{7/2}$	Dirac	1 433.228	1 498.105	1 498.114	1 564.452
	$E_{VP}^{(1)}$	3.697	3.972	3.972	4.258
	E_{LS}	−0.013	−0.015	−0.015	−0.016
	$E_{VP}^{(h)}$	−0.141	−0.156	−0.156	−0.172
	E_{RR}	0.005	0.005	0.005	0.006
	E_{ES}	0.138	0.153	0.153	0.170
	E_{NP}	0.0	0.0	0.0	0.0

TABLE VI. (Continued)

Level	Calculation	^{232}Th	^{235}U	^{238}U	^{239}Pu
$5g_{7/2}$	Dirac	919.022	960.707	960.713	1 003.345
	$E_{\rm VP}^{(1)}$	1.107	1.219	1.219	1.337
	$E_{\rm LS}$	0.005	0.006	0.006	0.006
	$E_{\rm VP}^{(h)}$	−0.081	−0.090	−0.090	−0.100
	$E_{\rm RR}$	0.002	0.002	0.002	0.002
	$E_{\rm ES}$	0.255	0.281	0.281	0.311
	$E_{\rm NP}$	0.0	0.0	0.0	0.0
$5g_{9/2}$	Dirac	915.013	956.326	956.332	998.566
	$E_{\rm VP}^{(1)}$	1.072	1.180	1.180	1.293
	$E_{\rm LS}$	−0.004	−0.005	−0.005	−0.005
	$E_{\rm VP}^{(h)}$	−0.080	−0.088	−0.088	−0.097
	$E_{\rm RR}$	0.002	0.002	0.002	0.002
	$E_{\rm ES}$	0.257	0.284	0.284	0.314
	$E_{\rm NP}$	0.0	0.0	0.0	0.0

Expression (11b) is a generalization of that given by Wilets[5] for $l=2$ and Acker[24] for $l=2$ and 4.

The uncorrected eigenvalues W obtained by numerically solving Eq. (2) are tabulated in Table VI for the $1s$, $2p$, $3d$, $4f$, and $5g$ muonic levels in ^{232}Th, ^{235}U, ^{238}U, and ^{239}Pu.

2. *Corrections to the Dirac solutions*

The Dirac solutions of Eq. (2) are not sufficiently accurate to describe the experimental measurements, even for a heavy spherical nucleus such as ^{208}Pb. Several corrections to the monopole Dirac solutions must be calculated in the process of calculating the eigenvalues of the muon-nucleus system (first order vacuum polarization, reduced mass correction, and Lamb shift) or added by using extrapolations of calculations of others (nuclear polarization, higher order vacuum polarization, relativistic recoil, and electron screening).

The largest correction, of the order of 75 keV in the $1s_{1/2}$ muon states of these actinide nuclei, is the first order vacuum polarization due to virtual emission and reabsorption of electron pairs. This leads to an energy shift of the form[25]

$$\Delta E_{\rm VP}^{(1)} = \int V_{\rm pol}(r)(F^2+G^2)dr \,, \tag{12}$$

with F and G defined by Eq. (2), while $V_{\rm pol}$ is the effective vacuum polarization potential

$$V_{\rm pol}(r) = (2\alpha/3\pi)[V_L(r) - \tfrac{5}{6}V_0(r)] \,. \tag{13}$$

Here $V_0(r)$ is given by Eq. (11a) and

$$V_L(r) = -(2\pi e^2/r)\int \rho(r')r'\left[|r-r'|\left(\ln\frac{1.781}{\lambda\!\!\!^{-}_e}|r-r'|-1\right) - (r+r')\left(\ln\frac{1.781}{\lambda\!\!\!^{-}_e}(r+r')-1\right)\right]dr' \,. \tag{14}$$

Higher order vacuum polarization terms are significant, especially in the $1s_{1/2}$ muon states. The values used in our analysis were interpolated from values calculated by Rinker and Wilets[26] at $Z=82$, 92, 98, and 114.

The Lamb shift in heavy muonic atoms is larger than experimental error, being of the order of 2–3 keV for the $1s_{1/2}$ states in these actinide nuclei. In our analysis this correction is calculated using an expression of Barrett *et al.*[27]:

$$\Delta E_{\rm LS} = (\alpha/\pi m^2)\left[\frac{1}{3}\langle\nabla^2 V\rangle\left(\ln\frac{m}{2\Delta\epsilon}+\frac{11}{24}+\frac{3}{8}-\frac{1}{5}\right) + \frac{1}{8}\left\langle\frac{2}{r}\frac{dV}{dr}\vec{\sigma}\cdot\vec{L}\right\rangle\right] \,. \tag{15}$$

The average excitation energy $\Delta\epsilon$ is defined by the Bethe sum and is of the order of 8–10 MeV and is discussed in detail by Barrett.[28] The term $-\frac{1}{5}$ is associated with the first order vacuum polarization term of the virtual muon pairs while

$$\langle\nabla^2 V\rangle = 4\pi Z\alpha\langle\rho\rangle \tag{16}$$

and is proportional to the overlap of the muon wave function with the nuclear charge distribution. The other terms are discussed in detail in Ref. 27.

Another large correction to the Dirac eigenvalues is nuclear polarization. A detailed discussion of this effect applied to deformed muonic atoms is given by Chen.[29] The values used in this work for the $1s_{1/2}$, $2p_{1/2}$, and $2p_{3/2}$ levels are taken, with suitable modifications, from Chen,[30] while the nuclear polarization values for the higher muonic levels are from Skardhamar,[31] again with suitable but minor modifications to apply to the Z and A values of interest here.

Electron screening and relativistic recoil corrections while small (less than 500 eV for the muonic atoms and levels considered here) can be calculated accurately[32] and have been included. The values for the first and higher order vacuum polarization, Lamb shift, nuclear polarization, electron screening, and relativistic recoil corrections used in the present analysis are listed in Table VI.

B. Quadrupole interaction and nuclear models

1. *Quadrupole matrix elements*

The nuclei of the muonic atoms of concern here have a stable, highly deformed shape with a large quadrupole moment, ~10 b. Thus, the second term of the potential expansion of Eq. (11) will make important contributions to the energy eigenvalues and will mix levels with different I, the nuclear spin, and j_μ, the muon spin, so that only their sum

$$\vec{F}=\vec{I}+\vec{j}_\mu \tag{17}$$

will be a good quantum number.

The quadrupole part of the potential is obtained from expression (11b) with $l=2$ and

$$\mathcal{E}_2=Q_0=\left(\frac{16\pi}{5}\right)^{1/2}\int \rho(r)r^2Y_{20}(\theta,\phi)d^3r\ , \tag{18}$$

so that

$$V_2(\vec{r}_\mu)=H_Q$$
$$=-\tfrac{1}{2}e^2Q_0f_2(r_\mu)\left(\frac{4\pi}{5}Y_{20}(\theta_\mu,\phi_\mu)Y_{20}(\theta_N,\phi_N)\right). \tag{19}$$

The operator H_Q is diagonalized in a basis whose state functions are

$$|IKnlj_\mu FM\rangle=\sum_{m_j}C(j_\mu IF;m_jM-m_jM)\times|nlj_\mu m_j\rangle|IM-m_jK\rangle\ , \tag{20}$$

where the $|nlj_\mu m_j\rangle$ are the Dirac solutions for the muon and the $|IM_IK\rangle$ are the nuclear state functions whose form depends upon the nuclear model. In this state function I is the total nuclear spin, K is its projection on the body-fixed 3 axis, and M is the projection on the laboratory Z axis. The matrix elements of $V_2(\vec{r}_\mu)$ are

$$\langle I_1K_1n_1l_1j_1FM|H_Q|I_2K_2n_2l_2j_2FM\rangle=\langle 1FM|H_Q|2FM\rangle$$
$$=-\frac{2\pi e^2}{5}Q_0(-1)^{j_2+I_2-F}[(2I_1+1)(2j_1+1)]^{1/2}W(j_1I_1j_2I_2;F2)$$
$$\times\langle I_1K_1||Y_{20}(\theta_N,\phi_N)||I_2K_2\rangle\langle j_1||f_2(r_\mu)Y_{20}(\theta_\mu,\phi_\mu)||j_2\rangle\ , \tag{21}$$

where $W(abcd;ef)$ is a Racah coefficient[21] and the double barred quantities are reduced matrix elements for the nuclear and muon operators. The muon reduced matrix element can be written as

$$e^2Q_0\langle j_1||f_2(r_\mu)Y_{20}(\theta_\mu,\phi_\mu)||j_2\rangle=(-1)^{1/2-l_2-j_2}[5(2l_1+1)(2j_2+1)/4\pi]^{1/2}$$
$$\times Q_0e^2C(l_12l_2;000)W(l_2j_2l_1j_1;\tfrac{1}{2}2)\langle l_1||f_2(r_\mu)||l_2\rangle\ , \tag{22}$$

where

$$Q_0e^2\langle l_1||f_2(r_\mu)||l_2\rangle$$
$$=Q_0e^2\int_0^\infty f_2(r)[F_1(r)F_2(r)+G_1(r)G_2(r)]dr$$
$$=-10\alpha_{j_1j_2}\ . \tag{23}$$

These reduced quadrupole radial matrix elements $\alpha_{j_1j_2}$ are tabulated in Table VII. Since H_Q is diagonalized only within the same muon shell ($n_1=n_2$), this table contains only α's belonging to the same l value ($j_{1,2}=l\pm\frac{1}{2}$).

2. *Nuclear models*

In order to evaluate the reduced nuclear matrix element of Eq. (21), some comments must be made concerning the nuclear model. Heavy deformed nuclei are relatively well described by a collective model and the choice here is for the simplest.[33] Any other model which adequately describes the level structure and the electric multipole moments will give similar results.

The ground state rotational band structures[34] for ^{232}Th, ^{235}U, ^{238}U, and ^{239}Pu are shown in Fig. 9. The quadrupole interaction H_Q couples these levels with the muonic levels giving rise through the dy-

TABLE VII. Matrix elements calculated from the fitted charge parameters.

Matrix element	^{232}Th	^{235}U	^{238}U	^{239}Pu
Dipole radial matrix elements (fm)				
$\langle 2p_{1/2}\Vert r\Vert 1s_{1/2}\rangle$	8.330	8.268	8.289	8.216
$\langle 2p_{3/2}\Vert r\Vert 1s_{1/2}\rangle$	8.608	8.554	8.575	8.509
$\langle 3d_{3/2}\Vert r\Vert 2p_{1/2}\rangle$	14.073	13.864	13.886	13.674
$\langle 3d_{3/2}\Vert r\Vert 2p_{3/2}\rangle$	14.518	14.287	14.304	14.072
$\langle 3d_{5/2}\Vert r\Vert 2p_{3/2}\rangle$	14.759	14.537	14.555	14.332
$\langle 4f_{5/2}\Vert r\Vert 3d_{3/2}\rangle$	27.507	26.861	26.865	26.245
$\langle 4f_{5/2}\Vert r\Vert 3d_{5/2}\rangle$	28.302	27.662	27.664	27.050
$\langle 4f_{7/2}\Vert r\Vert 3d_{5/2}\rangle$	28.597	27.964	27.966	27.359
$\langle 5g_{7/2}\Vert r\Vert 4f_{5/2}\rangle$	48.991	47.863	47.863	46.781
$\langle 5g_{7/2}\Vert r\Vert 4f_{7/2}\rangle$	49.443	48.325	48.324	47.253
$\langle 5g_{9/2}\Vert r\Vert 4f_{7/2}\rangle$	49.801	48.691	48.691	47.628
Quadrupole radial matrix elements (fm^2)				
$\langle 3d_{3/2}\Vert r^2\Vert 1s_{1/2}\rangle$	79.823	79.196	79.655	78.771
$\langle 3d_{5/2}\Vert r^2\Vert 1s_{1/2}\rangle$	81.413	80.849	81.316	80.493
$\langle 4f_{5/2}\Vert r^2\Vert 2p_{1/2}\rangle$	206.247	199.954	200.574	194.321
$\langle 4f_{5/2}\Vert r^2\Vert 2p_{3/2}\rangle$	225.764	218.711	219.237	212.309
$\langle 4f_{7/2}\Vert r^2\Vert 2p_{3/2}\rangle$	228.724	221.698	222.230	215.327
$\langle 5g_{7/2}\Vert r^2\Vert 3d_{3/2}\rangle$	812.740	774.937	775.137	739.699
$\langle 5g_{7/2}\Vert r^2\Vert 3d_{5/2}\rangle$	869.603	831.148	831.270	795.218
$\langle 5g_{9/2}\Vert r^2\Vert 3d_{5/2}\rangle$	876.699	838.243	838.365	802.311
Reduced quadrupole matrix elements (keV)				
$2p$: $\alpha_{1/2,3/2}$	80.644	90.627	94.662	101.655
$\alpha_{3/2,3/2}$	81.352	91.555	95.657	102.868
$3d$: $\alpha_{3/2,3/2}$	17.011	19.844	20.967	23.359
$\alpha_{5/2,3/2}$	14.896	17.325	18.325	20.356
$\alpha_{5/2,5/2}$	14.663	17.057	18.045	20.049
$4f$: $\alpha_{5/2,5/2}$	2.523	2.962	3.142	3.524
$\alpha_{7/2,5/2}$	2.352	2.752	2.920	3.264
$\alpha_{7/2,7/2}$	2.340	2.737	2.904	3.246
$5g$: $\alpha_{7/2,7/2}$	0.569	0.666	0.707	0.791
$\alpha_{9/2,7/2}$	0.550	0.643	0.682	0.762
$\alpha_{9/2,9/2}$	0.550	0.643	0.682	0.762
Reduced hexadecapole matrix elements (keV)				
$3d$: $\eta_{3/2,3/2}$	0.333	0.111	0.463	0.426
$\eta_{5/2,3/2}$	0.281	0.104	0.391	0.363
$\eta_{5/2,5/2}$	0.272	0.102	0.380	0.354
$4f$: $\eta_{5/2,5/2}$	0.018	0.009	0.026	0.026
$\eta_{7/2,5/2}$	0.015	0.008	0.022	0.022
$\eta_{7/2,7/2}$	0.015	0.008	0.022	0.022

TABLE VII. (Continued)

Matrix element	^{232}Th	^{235}U	^{238}U	^{239}Pu
	Reduced hexadecapole matrix elements (keV)			
$5g$: $\eta_{7/2,7/2}$	0.001	0.001	0.002	0.002
$\eta_{9/2,7/2}$	0.001	0.001	0.002	0.002
$\eta_{9/2,9/2}$	0.001	0.001	0.002	0.002

namic hyperfine interaction to a complicated coupled muon-nucleus system.

The reduced nuclear matrix elements of Eq. (21) are identical for both even-even and odd-A nuclei,[21,33]

$$\langle I_1K_1||Y_{20}(\theta_N,\phi_N)||I_2K_2\rangle = \left(\frac{5}{4\pi}\right)^{1/2} C(I_1 2 I_2; -K_1 0 -K_2)\delta_{K_1K_2} . \quad (24)$$

The ground state rotational band of even-even nuclei has $K=0$. For odd-A nuclei, not only is K not zero, but it is half an odd integer, a fact which introduces a great deal of complexity into the x-ray spectra as can be seen by a comparison of the even-even and odd-A spectra (Figs. 3–5).

Diagonalizing an interaction matrix for a given $|FMnl\rangle$ leads to mixed states of the form

$$|FMnl\rangle = \sum_{Ij} V_{FnlIj}|IKnlj_\mu FM\rangle . \quad (25)$$

The diagonalization process gives the amplitudes V_{FnlIj} of the components of the state functions as well as the energy eigenvalues E_{Finl}. Here i denotes the ordinal of the eigenvalue belonging to the state with total angular momentum F.

C. Other nuclear interactions

Several other muon-nucleus interactions may occur and these are discussed in order of their magnitude.

1. Hexadecapole, Y_4, interaction

A nonzero value for β_4 implies that the Y_4 interaction and the intrinsic moment will not be zero. (In general even if β_4 is identically zero the intrinsic hexadecapole moment will be nonzero and will indeed be positive for all values of β_2. Only if β_4 is negative can its associated intrinsic moment be zero or negative.) The matrix elements for this interaction can be written as a generalization of Eq. (21),

$$\langle 1FM|H_H|2FM\rangle = -9\eta_{j_1j_2}(-1)^{F-I_2-1/2+l_2}[(2I_1+1)(2j_1+1)(2l_1+1)(2j_2+1)]^{1/2}W(j_1I_1j_2I_2;F4)W(l_1j_1l_2j_2;\tfrac{1}{2}4) \times C(I_1 4 I_2; -K_1 0 -K_1)C(l_1 4 l_2; 000)\delta_{K_1K_2} , \quad (26)$$

where the $\eta_{j_1j_2}$ are the integrals over the appropriate generalized penetration function of Eq. (10):

$$\mathcal{E}_4e^2\langle l_1||f_4(r_\mu)||l_2\rangle = \mathcal{E}_4e^2\int_0^\infty f_4(r)[F_1(r)F_2(r) + G_1(r)G_2(r)]dr = -18\eta_{j_1j_2} . \quad (27)$$

The angular momentum factors of Eq. (26) dictate that the Y_4 interaction matrix elements vanish for muon states with $l<2$. The values of $\eta_{j_1j_2}$ for the hexadecapole interaction are tabulated in Table VII. While these are two orders of magnitude smaller than the $\alpha_{j_1j_2}$ of the quadrupole interaction, they have been included in the fitting procedure since their contribution to the interaction is of the same magnitude as the experimental uncertainty in the data.

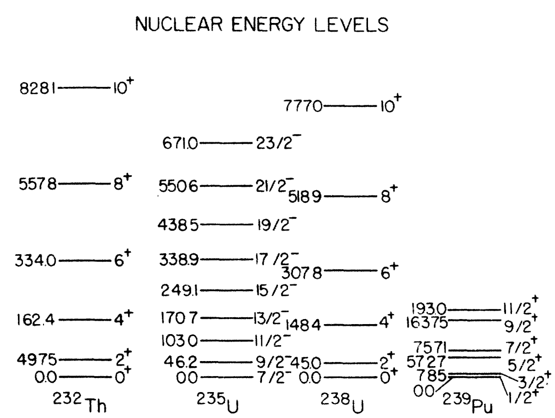

FIG. 9. The ground state rotational band with spins, parities, and energies in keV for those states used in the model to fit the ^{232}Th, ^{235}U, ^{238}U, and ^{239}Pu muonic data.

2. Magnetic hyperfine interaction

The magnetic hyperfine interaction occurs only for odd-A muonic atoms and has the form[1]

$$\Delta E_F(M1) = \frac{1}{2Ij}\,[F(F+1) - I(I+1) - j(j+1)]A_1\,. \tag{28}$$

The values of A_1 for ^{235}U and ^{239}Pu have been evaluated using the expression of LeBellac,[35] which are accurate enough for deformed nuclei with large quadrupole moments. The magnetic hyperfine interaction is smaller than the hexadecapole interaction and has not been included in the fitting of the odd-A data.

3. K-band mixing

The existence of other nuclear rotational bands of the same parity suggests the possibility that H_Q will connect nuclear states with different values of K[33,36] or with the same value of K but associated with a deformation vibration.[33,37] The relative importance of band mixing is proportional to the ratio of the bandhead energy to the energy of the first excited rotational state in the ground state band. In the even-even nuclei this ratio for the γ band ($K=2$) is 16 (^{232}Th) and 24 (^{238}U), while for the β band it is 15 and 22, respectively. For the odd-A nuclei, the nearest bands are not associated with the intrinsic particle ground state. In ^{235}U the nearest appropriate band is built on the $\frac{5}{2}^-[752]$ intrinsic state at 633.1 keV yielding a ratio of 14, while in ^{239}Pu the nearest band is built on a $\frac{5}{2}^+[622]$ state at 285.4 keV with a ratio of 36. For these actinide nuclei the contribution of K-band mixing to the muon-nucleus interaction is very small and has been ignored in the data analysis.

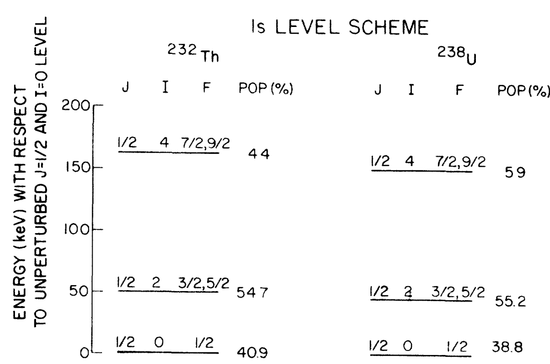

FIG. 10. Muonic 1s level scheme for ^{232}Th and ^{238}U. Each level is labeled by $J=\frac{1}{2}$, I, and F, the muon total angular momentum, the nuclear spin, and the total angular momentum, respectively. Each level is doubly degenerate in the latter quantum number since the magnetic dipole hyperfine splitting is not shown. All levels with a population greater than 1% are included.

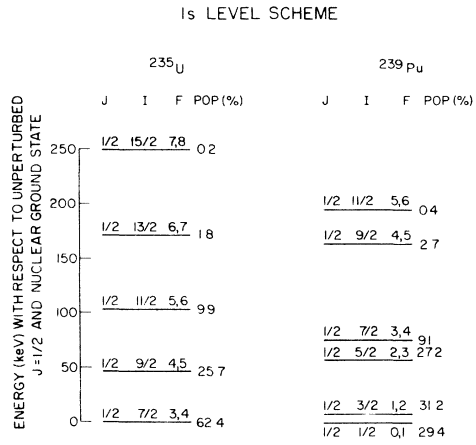

FIG. 11. Muonic 1s level scheme for ^{235}U and ^{239}Pu. Each level is labeled by $J=\frac{1}{2}$, I, and F, the muon total angular momentum, the nuclear spin, and the total angular momentum, respectively. Each level is doubly degenerate in the latter quantum number since the magnetic dipole hyperfine splitting is not shown. All levels with a population greater than 0.2% are included. The close doublet structure of ^{239}Pu is readily evident.

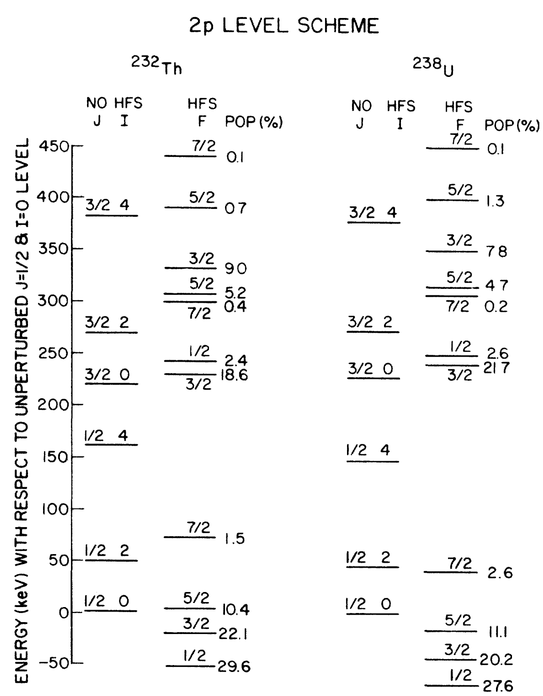

FIG. 12. Muonic 2p level scheme for ^{232}Th and ^{238}U. Levels with and without hyperfine splitting are shown. All levels with a population greater than 0.1% are included. The energy is relative to the unperturbed $J=\frac{1}{2}$ and $I=0$ muonic 2p level.

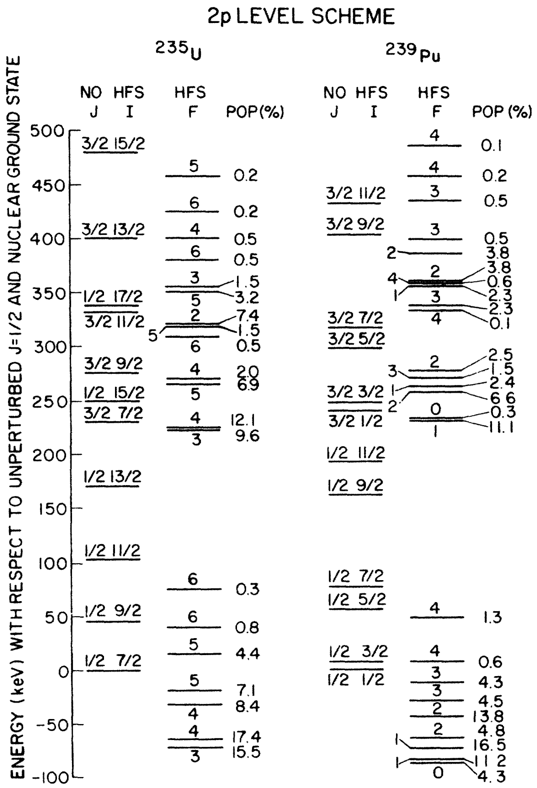

FIG. 13. Muonic $2p$ level scheme for ^{235}U and ^{239}Pu. Levels with and without hyperfine splitting are shown. All levels with a population of at least 0.1% are included. The energy is relative to the unperturbed muonic $2p_{1/2}$ level.

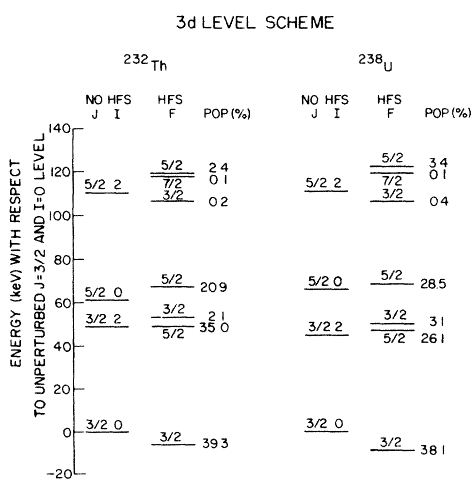

FIG. 14. Muonic $3d$ level scheme for ^{232}Th and ^{238}U. Levels with and without hyperfine splitting are shown. All levels with a population greater than 0.1% are included. The energy is relative to the unperturbed $J=\frac{3}{2}$ and $I=0$ muonic $3d$ level.

D. X-ray intensities

Once the eigenvalues $E_{F i n l}$ and the wave function amplitudes $V_{F n l I j}$ of Eq. (25) are known, the transition probabilities between any two levels can be calculated. The transition probability is proportional to

$$T(E\lambda) = \frac{|E_i - E_f|^{2\lambda+1}}{2F_i+1} \sum_{M_i M_f} |\langle F_f M_f n_f l_f | r^\lambda Y_{\lambda\sigma}(\theta,\phi) \times |F_i M_i n_i l_i\rangle|^2 \,. \tag{29}$$

Making use of angular momentum theorems, this expression can be reduced to

$$T(E\lambda) = |E_i - E_f|^{2\lambda+1}(2l_f+1)(2F_f+1)C^2(l_f\lambda l_i;000) \times \Bigg| \sum_{j_f j_i I} (-1)^{j_f+j_i-I+1/2}\delta_{A,\mathrm{odd}}[(2j_1+1)(2j_f+1)]^{1/2} \times V_{F_f n_f l_f I j_f} V_{F_i n_i l_i I j_i} \langle l_f \| r_\mu^\lambda \| l_i\rangle \times W(l_f j_f l_i j_i;\tfrac{1}{2}\lambda) W(j_f j_i F_f F_i;\lambda I)\Bigg|^2 \tag{30}$$

The reduced matrix element is

$$\langle l_f \| r_\mu^\lambda \| l_i\rangle = \int_0^\infty r^\lambda [F_f(r)F_i(r) + G_f(r)G_i(r)]dr \,. \tag{31}$$

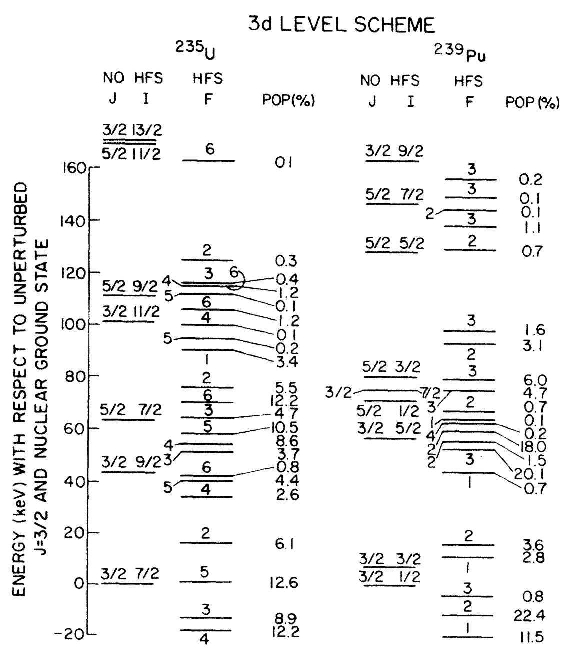

FIG. 15. Muonic $3d$ level scheme for ^{235}U and ^{239}Pu. Levels with and without hyperfine splitting are shown. All levels with a population of at least 0.1% are included. The energy is relative to the unperturbed muonic $3d_{3/2}$ level.

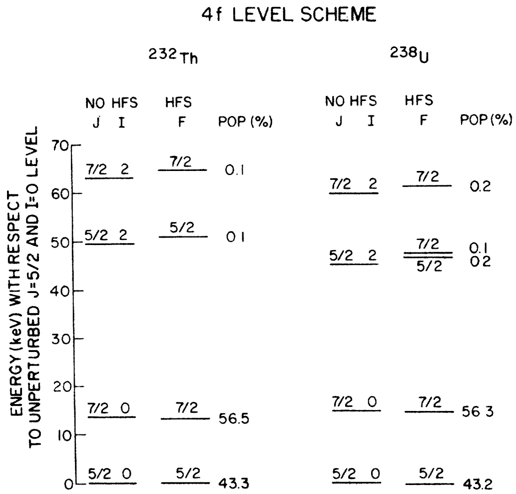

FIG. 16. Muonic $4f$ level scheme for ^{232}Th and ^{238}U. Levels with and without hyperfine splitting are shown. All levels with a population greater than 0.1% are included. The energy is relative to the unperturbed $J=\frac{5}{2}$ and $I=0$ muonic $4f$ level.

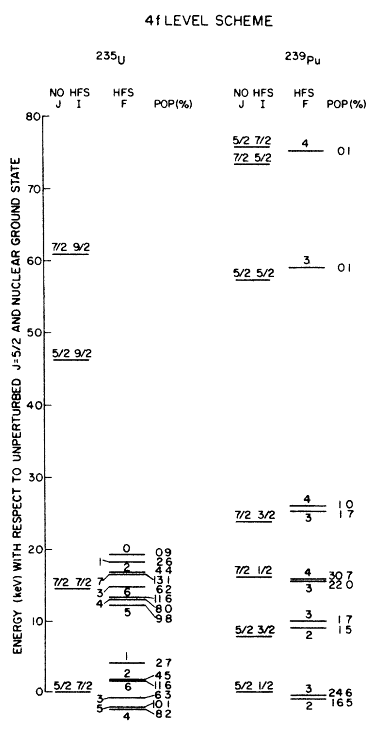

FIG. 17. Muonic $4f$ level scheme for ^{235}U and ^{239}Pu. Levels with and without hyperfine splitting are shown. All levels with a population of at least 0.1% are included. The energy is relative to the unperturbed muonic $4f_{5/2}$ level.

Some of these matrix elements for $\lambda = 1, 2$ calculated for the fitted parameters are listed in Table VII.

The relative muonic x-ray intensities of the principal lines are then calculated by multiplying the transition probability by the relative population of the initial state. The relative populations are determined by a cascade calculation linking only the "circular" orbits and starting in the $5g$ levels, assuming the nucleus is in its ground state and the quadrupole interaction can be neglected. The initial $5g$ level populations are assumed to be statistical while the others are calculated in the process of the cascade calculation. These populations are shown in Figs. 10–17.

V. ANALYSIS TECHNIQUE

The experimental transition energies of the $2p$-$1s$ and $3d$-$2p$ muonic x rays (specifically those marked with an asterisk in Tables II–V) were used to determine the charge distribution parameters of Eq. (8). Due to the strong quadrupole interaction present in these highly deformed nuclei, calculations yield a large multiplicity of transition energies, and some approach was necessary to provide a comparison between calculated and measured energies. The theoretical and experimental relative intensities were used to match the calculated and measured transition energies. We did not fit to the relative intensities because they were not measured with an accuracy comparable to that of the transition energies, and the calculated relative intensities and energies are not completely independent. In addition, an earlier analysis[22] in the rare-earth region showed an abnormally high contribution to χ^2 due to the intensities. We also did not fit to a measured quadrupole moment. Due to its low statistical weight, its inclusion would not significantly alter the results. No attempt was made to correct for the isotopic impurity of ^{235}U and ^{239}Pu, see Table I, when analyzing the data.

The actual fitting was done using a generalized least squares fitting routine LSMFT,[38] available through the Central Computing Facility of the Los Alamos Scientific Laboratory. The muonic x-ray transition energies were calculated and compared with the experimental energies, and the charge distribution parameters were varied until χ^2 was minimized. The least squares program considers correlations between parameters and evaluates the error matrix in order to calculate the uncertainties associated with the fitted parameters. Because of strong correlations and anticorrelations between the parameters,[17] it is not possible, as is often done, to determine the standard deviations of the parameters by altering each parameter independently until χ^2 changes by a fixed amount.

The higher dipole transitions between circular orbits, $4f$-$3d$ and $5g$-$4f$, the dipole transitions between noncircular orbits, $3p$-$1s$, $4d$-$2p$, and $5f$-$3d$, and the electric quadrupole transitions, $3d$-$1s$, $4f$-$2p$, and $5g$-$3d$, were not used to determine the charge distribution parameters. However, after the parameters were deduced from fitting the $2p$-$1s$ and $3d$-$2p$ transitions, these additional transition energies and relative intensities for the above transitions between circular orbits were calculated and compared with the experimental results to assure agreement. The calculated results for the dipole transitions ($4f$-$3d$ and $5g$-$4f$) are given in Tables II-V for each of the nuclei studied. The quadrupole transitions were calculated for ^{232}Th and ^{238}U, and these results are compared to the experiment in Figs. 6-8.

VI. ANALYSIS RESULTS

Table VIII presents the nuclear parameters which result from the fit to the muonic $2p$-$1s$ and $3d$-$2p$ transition energies for the four actinide nuclei ^{232}Th, ^{235}U, ^{238}U, and ^{239}Pu.

A preliminary analysis[2] of ^{232}Th and ^{238}U reported nonzero values for β_4. It also indicated[2] that nonzero values of β_6 were required by the data. The earlier analysis included only the $2p$-$1s$ transitions and represented a local minimum in χ^2 space. The present analysis using a more sophisticated search routine[38] is an improved analysis using the $2p$-$1s$ and $3d$-$2p$ transitions and results in a deeper minimum in χ^2 space. The present analysis shows no evidence for a nonzero β_6. In fact, the χ^2 obtained for β_4 identically zero is not significantly larger than the χ^2 obtained when β_4 is permitted to take on nonzero values.

The parameter a is very nearly constant for these nuclei, indicating that the skin thickness ($4a\ln 3$) is also constant to within ±1%. While the half density radius c increases with A over this very narrow region, it too is essentially constant.

Figures 10–17 show the muonic level schemes and the relative populations for the $1s$, $2p$, $3d$, and $4f$ muonic levels in ^{232}Th, ^{235}U, ^{238}U, and ^{239}Pu. These populations were determined by the cascade calculation described in Sec. IV D. The $1s$ muonic level scheme (Figs. 10 and 11) shows the populations of the nuclear levels for the four actinides. The populations for ^{232}Th and ^{238}U (Fig. 10) are very similar to each other, but both are quite different from ^{235}U and ^{239}Pu (Fig. 11). The ground state and first excited state of the even-even nuclei are about equally populated by the time the muon reaches the $1s$ state and together they are populated about 95% of the time. The higher excited states are very weakly populated. On the other hand, the ^{239}Pu ground state and first two excited states are each populated about 30% of the time, with the nucleus being left in the first excited state slightly more often than in either the ground state or the second excited state. The doublet structure of ^{239}Pu is readily evident and arises from a relatively large rotational decoupling parameter. The populations for ^{235}U are quite different from those for ^{239}Pu. The ground state is populated more than 60% of the time and the first excited state about 25% of the time.

Figures 12 and 13 show the $2p$ level schemes for ^{232}Th and ^{238}U and for ^{235}U and ^{239}Pu, respectively. The $2p$ level schemes show the fine structure splitting between the $2p_{1/2}$ and $2p_{3/2}$ levels in all four nuclei. The $2p$ hyperfine splittings in the even-even nuclei are very similar (Fig. 12), and the spectra for the $2p$-$1s$ transitions are also very similar (Fig. 3). The populations of the $2p_{1/2}$ and $2p_{3/2}$ fine structure components are about the same for ^{232}Th and ^{238}U.

The hyperfine splitting in the $2p$ level in ^{239}Pu is

TABLE VIII. Nuclear parameters resulting from the fit to the experimental muonic $2p$-$1s$ and $3d$-$2p$ transition energies.

	^{232}Th	^{235}U	^{238}U	^{239}Pu
a (fm)	0.449 ± 0.004	0.454 ± 0.006	0.448 ± 0.004	0.447 ± 0.014
c (fm)	7.024 ± 0.006	7.043 ± 0.008	7.076 ± 0.006	7.091 ± 0.016
β_2	0.252 ± 0.002	0.272 ± 0.002	0.279 ± 0.002	0.286 ± 0.002
β_4	0.001 ± 0.012	−0.026 ± 0.008	0.001 ± 0.012	−0.008 ± 0.018
Q_0 (b)	9.61 ± 0.07	10.51 ± 0.06	11.15 ± 0.05	11.66 ± 0.11
π_0 (b^2)	0.73 ± 0.06	0.34 ± 0.02	0.95 ± 0.09	0.85 ± 0.16
χ^2	10.9	23.9	23.8	16.1

more complicated than that for ^{235}U (Fig. 13). This predicts that the $2p$-$1s$ transition in ^{239}Pu is more complicated than the same transition in ^{235}U. A look at Fig. 3 clearly shows this is the case. While the ^{239}Pu $2p$ level is more fractured than the ^{235}U $2p$ level, the populations of the states in the $2p$ fine structure groups are roughly the same for both odd-A nuclei. Again, the doublet structure of ^{239}Pu is evident.

The $3d$ level schemes for the even-even nuclei are shown in Fig. 14. There is no definite fine structure splitting between the $3d_{3/2}$ states and the $3d_{5/2}$ states. As is to be expected, the $3d$ level schemes in ^{232}Th and ^{238}U are very similar.

In contrast to the $2p$ level scheme in ^{235}U and ^{239}Pu, the $3d$ level in ^{235}U is more highly fractured than the $3d$ level in ^{239}Pu (Fig. 15). In these two odd-A nuclei, as in the even-even nuclei, there is no clear fine structure splitting of the $3d_{3/2}$ states from the $3d_{5/2}$ states.

The $4f$ muonic state is far removed from the nucleus so there should not be much hyperfine splitting. Figure 16, which displays the $4f$ level scheme in ^{232}Th and ^{238}U, shows there is basically no hyperfine splitting in these even-even nuclei. The $4f$ fine structure splitting is almost identical in ^{232}Th and ^{238}U. Figure 17 shows the $4f$ level scheme in ^{235}U and ^{239}Pu. The ^{235}U $4f$ level is more highly fractured than the ^{239}Pu $4f$ level.

The 5-3 muonic x-ray transitions in ^{232}Th and ^{238}U, Fig. 6, are characterized by three doublets not fully resolved. Also shown are the calculated energies and relative intensities for the $5g$-$3d$ quadrupole transitions. The theoretical calculations seem to explain the higher energy, lower intensity component of each doublet. The unperturbed $5g$-$5f$ separations for ^{232}Th and ^{238}U were calculated, and they appear to explain the observed splitting in each of the doublets. The lower energy component of each doublet is thus identified as the $5f$-$3d$ dipole transition.

The 4-2 muonic x-ray transitions for ^{232}Th and ^{238}U, Fig. 7, are also characterized by three sets of doublets, with the separation of the highest energy doublet being about twice that of the other two doublets. Also shown are the calculated energies and relative intensities for the $4f$-$2p$ quadrupole transitions. These quadrupole transitions nicely explain the higher energy component of each doublet. The unperturbed $4f$-$4d$ separations in ^{232}Th and ^{238}U have been calculated, and they account for the observed splitting in the doublets.

Figure 8 shows the $3d$-$1s$ experimental spectra and the calculated $3d$-$1s$ quadrupole transition energies and relative intensities for ^{232}Th and ^{238}U. The agreement is quite reasonable. The calculated $3p$-$1s$ dipole transition energies indicate that these transitions are significantly higher in energy than the $3d$-$1s$ transitions and cannot account for the observed structure. In ^{208}Pb we also saw[17] that the $3d$-$1s$ quadrupole transitions were lower in energy and stronger in intensity than the $3p$-$1s$ dipole transitions.

VII. DISCUSSION

From inspecting Tables II–V, it is seen that the calculated $4f$-$3d$ x-ray energies are not in good agreement with the experimentally measured $4f$-$3d$ x-ray energies; the calculated energies are 0.3–1.0 keV too low. This discrepancy is most obvious in ^{232}Th and ^{238}U and to a lesser extent in ^{239}Pu. Any possible discrepancy between the calculated and experimental $4f$-$3d$ x-ray energies in ^{235}U is hidden by the multitude of calculated $4f$-$3d$ x rays. Some data fits were performed which included the $4f$-$3d$ transition energies. Even when these $4f$-$3d$ transition energies were included, these data could not be fitted. This was true whether β_4 was identically zero or was allowed to vary. Two additional calculations were performed in an effort to improve the comparison to the $4f$-$3d$ x rays in ^{232}Th and ^{238}U.

First, the energy of the first excited state in ^{232}Th and ^{238}U was varied by 0.5 keV. An inspection of Fig. 14 shows the 2^+ state in ^{232}Th and ^{238}U to be important in the hyperfine structure in the muonic $3d$ states. These calculations used the charge distribution parameters previously determined (Table VIII) and the higher order corrections

TABLE IX. The effect on χ^2 for the $5g$-$4f$, $4f$-$3d$, $3d$-$2p$, and $2p$-$1s$ x rays when the energy of the first excited nuclear state in ^{232}Th and ^{238}U is lowered by 0.5 keV.

	^{232}Th		^{238}U	
	$E(2^+) = 49.75$ keV	$E(2^+) = 49.25$ keV	$E(2^+) = 45.0$ keV	$E(2^+) = 44.5$ keV
χ^2_{5g-4f}	3.2	3.1	6.9	7.3
χ^2_{4f-3d}	105.5	51.0	198.1	70.6
χ^2_{3d-2p}	3.9	6.1	6.7	6.3
χ^2_{2p-1s}	7.0	7.3	17.1	17.6

TABLE X. The χ^2 for the $5g$-$4f$, $4f$-$3d$, $3d$-$2p$, and $2p$-$1s$ x rays in ^{232}Th and ^{238}U using the adjusted nuclear polarizations.

	^{232}Th	^{238}U
χ^2_{5g-4f}	0.0	0.0
χ^2_{4f-3d}	11.3	10.5
χ^2_{3d-2p}	5.0	13.7
χ^2_{2p-1s}	7.4	20.0
Muonic level	^{232}Th Adjusted nuclear polarization (keV)	^{238}U Adjusted nuclear polarization (keV)
$1s_{1/2}$	6.6	6.5
$2p_{1/2}$	2.4	1.9
$2p_{3/2}$	2.3	2.3
$3d_{3/2}$	0.3	0.3
$3d_{5/2}$	0.8	0.3
$4f_{5/2}$	0.02	−0.1
$4f_{7/2}$	0.01	−0.2

and nuclear polarization corrections to the muonic levels listed in Table VI. A decrease in the energy of the 2^+ nuclear state by 0.5 keV raises the calculated $4f$-$3d$ x-ray energies 0.2–0.5 keV. This increase in the calculated $4f$-$3d$ x-ray energies reduces the $4f$-$3d$ x-ray χ^2 by more than a factor of 2. Table IX summarizes these calculations for ^{232}Th and ^{238}U. There are no significant changes in χ^2 for the $2p$-$1s$, $3d$-$2p$, and $5g$-$4f$ x rays. The $3d$-$2p$ x-ray χ^2 for ^{232}Th increases by about 60%, but the total χ^2 is still quite reasonable.

This result led us to see if the ground state rotational band energies in ^{232}Th and ^{238}U had been remeasured since those reported in Ref. 34. Recent experiments [39–41] have measured the energy of these 2^+ states and have found them to be 0.1–0.4 keV lower than the values used in the present analysis. These newer values are still within the energy uncertainties (a few keV) quoted in the Nuclear Data Tables.[34]

The second set of calculations varied the nuclear polarizations of the muonic levels, keeping the charge distribution parameters fixed at the previously determined values (Table VIII) and using the accepted energy level schemes (Fig. 9). It is reasonable to assume that the higher order vacuum polarization, relativistic recoil, and electron screening calculations are more accurate than the nuclear polarization calculations. The nuclear polarizations used for the $1s_{1/2}$, $2p_{1/2}$, and $2p_{3/2}$ muonic levels were extrapolated from Ref. 30. The nuclear polarizations for the $3d_{3/2}$ and $3d_{5/2}$ muonic levels were those calculated by Skardhamar[31] for the spherical, even-even nucleus ^{208}Pb. There is no *a priori* reason to assume that these are correct for the highly deformed actinide nuclei. Additionally, Skardhamar did not calculate nuclear polarizations above the $3d_{5/2}$ level.

For these calculations, the nuclear polarizations for the $5g_{7/2}$ and $5g_{9/2}$ levels were assumed to be zero. The $4f$ nuclear polarizations were adjusted until the calculated and experimental $5g$-$4f$ x-ray energies agreed. Next, the $3d$ nuclear polarizations were varied until the χ^2 for the $4f$-$3d$ x rays was minimized. Then the $3d$-$2p$ x-ray χ^2 was minimized varying the $2p$ nuclear polarizations. Finally, the $1s$ nuclear polarization was varied until the $2p$-$1s$ x-ray χ^2 was minimized. The results of this procedure for ^{232}Th and ^{238}U are presented in Table X. For these two even-even nuclei, there is a significant decrease in the χ^2 for the $4f$-$3d$ x rays—an order of magnitude. The χ^2 for the $3d$-$2p$ and $2p$-$1s$ x rays generally showed only minor changes when the new nuclear polarizations were used. In contrast to the earlier work[17] on the spherical nucleus ^{208}Pb, no indication is seen that the calculated nuclear polarization for the $1s_{1/2}$ muonic level in these two highly deformed even-even actinide nuclei is small by about a factor of 2.

An identical analysis was performed on ^{239}Pu. Only a small improvement in the fit to the $4f$-$3d$ x rays was achieved when the nuclear polarizations were adjusted.

Due to the differences in the form of the models

TABLE XI. Comparison of quadrupole moments (in barns) deduced from muonic x ray measurements.

Nucleus	CERN [a]	Chicago [b]	Carnegie [c]	Present work
^{232}Th	9.80 ± 0.30	9.83 ± 0.16	9.70 ± 0.13	9.61 ± 0.07
^{235}U	10.60 ± 0.20	···	···	10.51 ± 0.06
^{238}U	11.25 ± 0.15	11.47 ± 0.13	11.30 ± 0.11	11.15 ± 0.05
^{239}Pu	12.00 ± 0.30	···	···	11.66 ± 0.11

[a] See Ref. 11. [b] See Ref. 12. [c] See Ref. 13.

TABLE XII. Comparison of deformation parameters for ^{232}Th and ^{238}U as deduced from electron, proton, α inelastic scattering and muonic x rays.

Nucleus	Parameter	NBS [a] 35–110 MeV electrons	Saclay [b] 23 MeV protons	Berkeley [c] 50 MeV α particles	ORNL [d] 16–18 MeV α particles	Pittsburgh [e] 16.5 and 17 MeV α particles	Los Alamos muonic x rays
^{232}Th	β_2	0.238	0.230	···	0.238	0.232	0.252
	β_4	0.101	0.050	···	0.130	0.123	0.001
	β_6	0.0	0.0	···	0.0	0.0	0.0
^{238}U	β_2	0.261	0.270	0.220	0.283	···	0.279
	β_4	0.087	0.017	0.060	0.059	···	0.001
	β_6	0.0	−0.015	−0.012	0.0	···	0.0

[a] See Ref. 42.
[b] See Ref. 43.
[c] See Ref. 44.
[d] See Ref. 45.
[e] See Ref. 46.

used for the nuclear charge distributions, it is not possible to directly compare these nuclear shapes with those from earlier muonic x-ray experiments. However, Table XI shows the good agreement that exists for the quadrupole moments which are deduced from the various muonic x-ray studies.

The deformation parameters of ^{232}Th and ^{238}U have been studied using electron,[42] proton,[43] and α[44–46] inelastic scattering. These results are shown in Table XII together with our muonic x-ray results. The β_2 values derived from the scattering experiments on ^{232}Th are in good agreement while there is a considerable spread of values for ^{238}U. Each of the scattering experiments requires a nonzero value for β_4 for both ^{232}Th and ^{238}U. However, there is little overall agreement on the value of β_4 from the various scattering experiments. Our β_2 values are larger than most values from inelastic scattering. (This, however, is presumably due to the fact that our analysis required $\beta_4 = 0$. In the fits to the muonic data the correlation of parameters is such that positive values of β_4 would result in a reduced value for β_2.) We have attempted to fit our muonic x-ray data with each set of deformation parameters determined by inelastic scattering, allowing the half density radius and diffuseness parameters, c and a, to vary. A significantly poorer fit was obtained in each case. Although the fit was poor, the inelastic electron scattering deformation parameters produced better agreement with our data than the parameters from proton and α scattering. This may be due to the electron and muon being electromagnetic probes while the heavy charged particles may be influenced by the nuclear potential. This analysis adds further experimental support to the arguments of Madsen, Brown, and Anderson[47] that the quadrupole deformation parameter may be dependent upon the probing particle.

ACKNOWLEDGMENTS

The authors wish to recognize the advice and assistance given by R. E. Welsh and R. J. Powers during the planning of this experiment. R. T. Siegel and the SREL staff provided efficient operation of the facility which made the experiment possible. The help and assistance of C. J. Umbarger, L. V. East, and R. H. Augustson during the planning and data taking phase of this work is gratefully appreciated. We wish to thank D. V. Susco, R. J. Beckman, and C. McInteer for helping us to implement the fitting routine LSMFT. One of us (JPD) wishes to acknowledge the partial support by the Los Alamos Scientific Laboratory and the Associated Western Universities, Inc., during his sabbatical leave year (1974–1975).

†Work performed under the auspices of the U. S. Energy Research and Development Administration.
*On sabbatical leave from the University of Kansas, Lawrence, Kansas 66045, 1974–1975 academic year.
[1] C. S. Wu and L. Wilets, Annu. Rev. Nucl. Sci. 19, 577 (1969), and references therein.
[2] J. P. Davidson, D. A. Close, and J. J. Malanify, Phys. Rev. Lett. 32, 337 (1974).
[3] D. A. Close, J. J. Malanify, and J. P. Davidson, presented at the Sixth International Conference on High Energy Physics and Nuclear Structure, Santa Fe and Los Alamos, New Mexico, June 9–14, 1975 (unpublished).
[4] R. J. Powers, F. Boehm, P.Vogel, A. Zehnder, T. King, A. R. Kunselman, P. Roberson, P. Martin, G. H. Miller, R. E. Welsh, and D. A. Jenkins, Phys. Rev. Lett. 34, 492 (1975); R. J. Powers, F. Boehm, P. Vogel, A. Zehnder, T. King, A. R. Kunselman, P. Roberson, P. Martin, G. H. Miller, R. E. Welsh, and D. A. Jenkins, Nucl. Phys. A262, 493 (1976).

[5]L. Wilets, Kgl. Dan. Viden. Selsk. Mat.-Fys. Medd. 29, No. 3 (1954).
[6]B. A. Jacobsohn, Phys. Rev. 96, 1637 (1954).
[7]R. D. Ehrlich, R. J. Powers, V. L. Telegdi, J. A. Bjorkland, S. Raboy, and C. C. Trail, Phys. Rev. Lett. 13, 550 (1964).
[8]H. L. Acker, H. Marschall, G. Backenstoss, and D. Quitmann, Nucl. Phys. 62, 477 (1965).
[9]S. Raboy, C. C. Trail, J. A. Bjorkland, R. D. Ehrlich, R. J. Powers, and V. L. Telegdi, Nucl. Phys. 73, 353 (1965).
[10]H. L. Acker, G. Backenstoss, C. Daum, J. C. Sens, and S. A. DeWit, Phys. Lett. 14, 317 (1965).
[11]S. A. DeWit, G. Backenstoss, C. Daum, J. C. Sens, and H. L. Acker, Nucl. Phys. 87, 657 (1967).
[12]R. J. McKee, Phys. Rev. 180, 1139 (1969).
[13]R. E. Coté, W. V. Prestwich, A. K. Gaigalas, S. Raboy, C. C. Trail, R. A. Carrigan, Jr., P. D. Gupta, R. B. Sutton, M. N. Suzuki, and A. C. Thompson, Phys. Rev. 179, 1134 (1969).
[14]Preliminary reports of this work are to be found in Refs. 2 and 3.
[15]H. O. Funsten, Nucl. Instrum. Methods 94, 443 (1971).
[16]J. T. Routti and S. G. Prussin, Nucl. Instrum. Methods 72, 125 (1969).
[17]D. A. Close, J. J. Malanify, and J. P. Davidson, Nuovo Cimento 34A, 301 (1976).
[18]R. L. Heath, Aerojet Nuclear Report No. ANCR-1000-2, March 1974 (unpublished).
[19]J. J. Malanify, R. H. Augustson, D. A. Close, L. V. East, and C. J. Umbarger, Trans. Am. Nucl. Soc. 16, 66 (1973).
[20]M. E. Rose, *Relativistic Electron Theory* (Wiley, New York, 1961).
[21]The definitions of spherical harmonics and angular momentum quantities follow M. E. Rose, *Elementary Theory of Angular Momentum* (Wiley, New York, 1957).
[22]D. Hitlin, S. Bernow, S. Devons, I. Duerdoth, J. W. Kast, E. R. Macagno, J. Rainwater, C. S. Wu, and R. C. Barrett, Phys. Rev. C 1, 1184 (1970).
[23]Y. N. Kim, *Mesic Atoms and Nuclear Structure* (North-Holland, Amsterdam, 1971), Chap. 3, Sec. 2.2.
[24]H. L. Acker, Nucl. Phys. 87, 153 (1966).
[25]K. W. Ford and J. G. Wills, Nucl. Phys. 35, 295 (1962).
[26]G. A. Rinker and L. Wilets, Phys. Rev. A12, 748 (1975).
[27]R. C. Barrett, S. J. Brodsky, G. W. Erickson, and M. H. Goldhaber, Phys.Rev. 166, 1589 (1968).
[28]R. C. Barrett, Phys. Lett. 28B, 93 (1968).
[29]M. Y. Chen, Phys. Rev. C 1, 1176 (1970).
[30]M. Y. Chen, Ph.D. thesis, Princeton University, 1968 (unpublished).
[31]H. F. Skardhamar, Nucl. Phys. A151, 154 (1970).
[32]We wish to thank G. A. Rinker for the use of his computer code to calculate the relativistic recoil and electron screening corrections.
[33]J. P. Davidson, *Collective Models of the Nucleus* (Academic Press, New York, 1968).
[34]M. R. Schmorak, Nucl. Data B4, 561 (1970); A. Artna-Cohen, *ibid*. B6, 287 (1971); Y. A. Ellis, *ibid*. B4, 635 (1970); A. Artna-Cohen, *ibid*. B6, 577 (1971).
[35]L. LeBellac, Nucl. Phys. 40, 645 (1963).
[36]M. Ikeda, A. Ikeda, and R. K. Sheline, Phys. Lett. B45, 187 (1973).
[37]G. Kanatas and J. P. Davidson, Nucl. Phys. A180, 638 (1972).
[38]R. H. Moore and R. K. Zeigler, Los Alamos Scientific Laboratory Report No. LA-2367, March 1960 (unpublished).
[39]W.R. McMurray and I. J. van Heerden, Z. Phys. 253, 289 (1972).
[40]M. Schmorak, C. E. Bemis, Jr., M. J. Zender, N. B. Gove, and P. F. Dittner, Nucl. Phys. A178, 410 (1972).
[41]B. B. Back, E. R. Flynn, O. Hansen, R. F. Casten, and J. D. Garrett, Nucl. Phys. A217, 116 (1973).
[42]T. Cooper, W. Bertozzi, J. Heisenberg, S. Kowalski, W. Turchinetz, C. Williamson, L. Cardman, S. Fivozinsky, J. Lightbody, Jr., and S. Penner, Phys. Rev. C 13, 1083 (1976).
[43]J. M. Moss, Y. D. Terrien, R. M. Lombard, C. Brassard, J. M. Loiseaux, and F. Resmini, Phys. Rev. Lett. 26, 1488 (1971).
[44]D. L. Hendrie, B. G. Harvey, J. R. Meriwether, J. Mahoney, J. C. Faivre, and D. G. Kovar, Phys. Rev. Lett. 30, 571 (1973).
[45]C. E. Bemis, Jr., F. K. McGowan, J. L. C. Ford, Jr., W. T. Milner, P. H. Stelson, and R. L. Robinson, Phys. Rev. C 8, 1466 (1973).
[46]C. Baktash and J. X. Saladin, Phys. Rev. C 10, 1136 (1974).
[47]V. A. Madsen, V. R. Brown, and J.D. Anderson, Phys. Rev. C 12, 1205 (1975); Phys. Rev. Lett. 34, 1398 (1975).